Introduction to Gamma-ray Burst Astrophysics

Jakub Řípa
Astronomical Institute of Charles University
MTA-Eötvös Loránd University, Budapest

Host Galaxies of GRBs and Core-Collapse SNe

- Hosts of LGRBs have systematically lower metalicities than either SNe hosts or general star-forming galaxies.

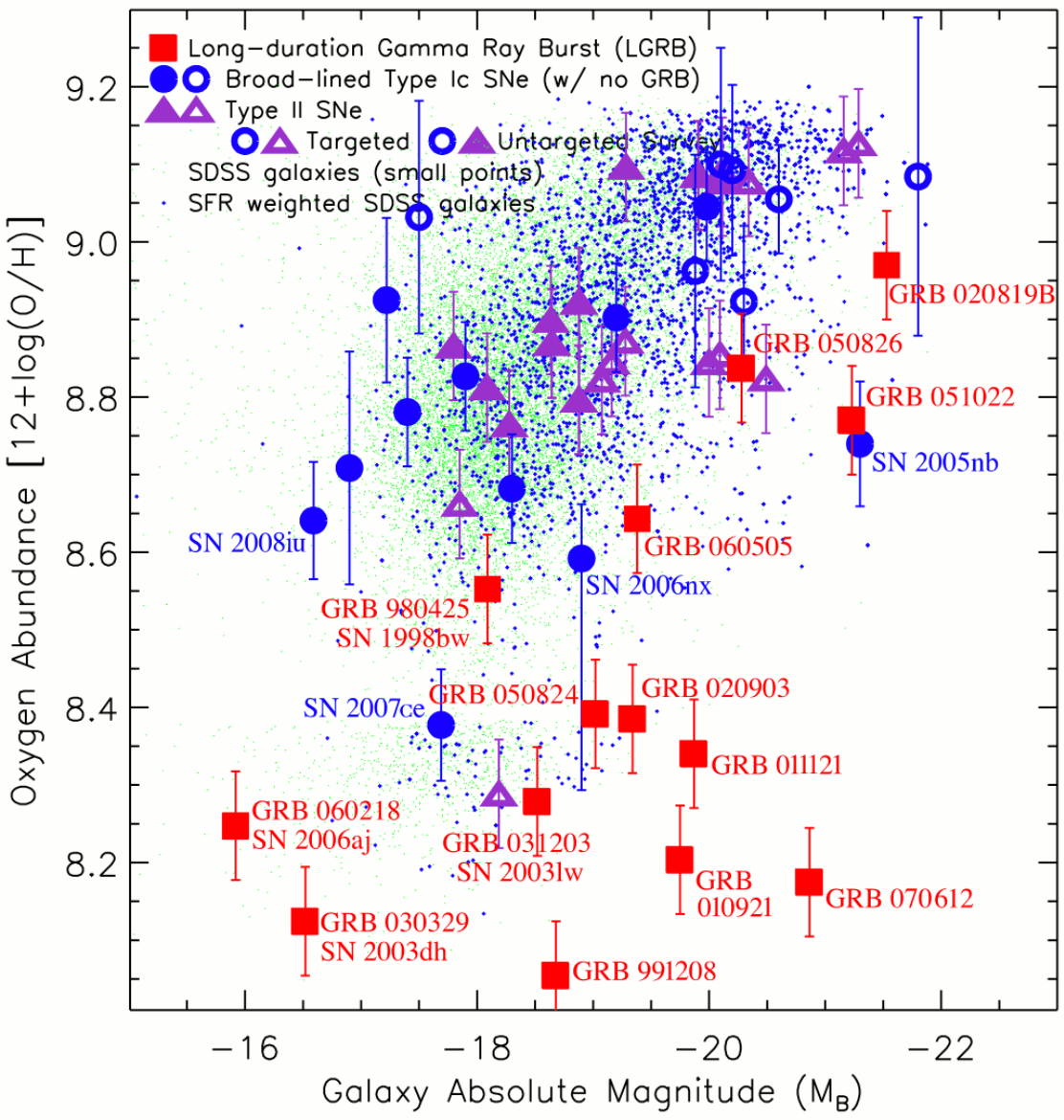

Graham and Fruchter 2013

Short vs Long GRBs

Short vs Long GRBs

- SGRBs have dimmer optical and X-ray afterglows than LGRBs.

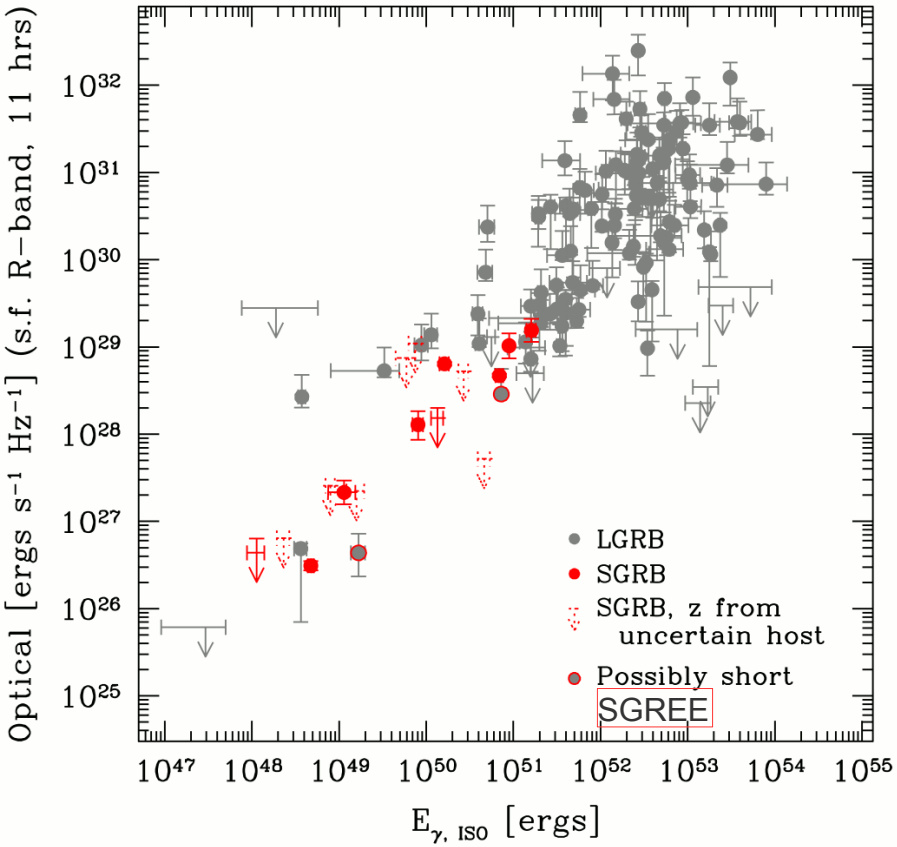

Figure 5. Rest-frame optical *R*-band (corrected for Galactic extinction) afterglow brightness at 11 hr (in the source frame) vs. $E_{\gamma,\mathrm{ISO}}$, the total prompt emission of the burst in gamma-rays. The dashed upper limits represent SGRBs with a host galaxy determined by XRT error circle only. The classification of GRB 060614 and GRB 060505 is uncertain, therefore they are labeled as "Possibly short."

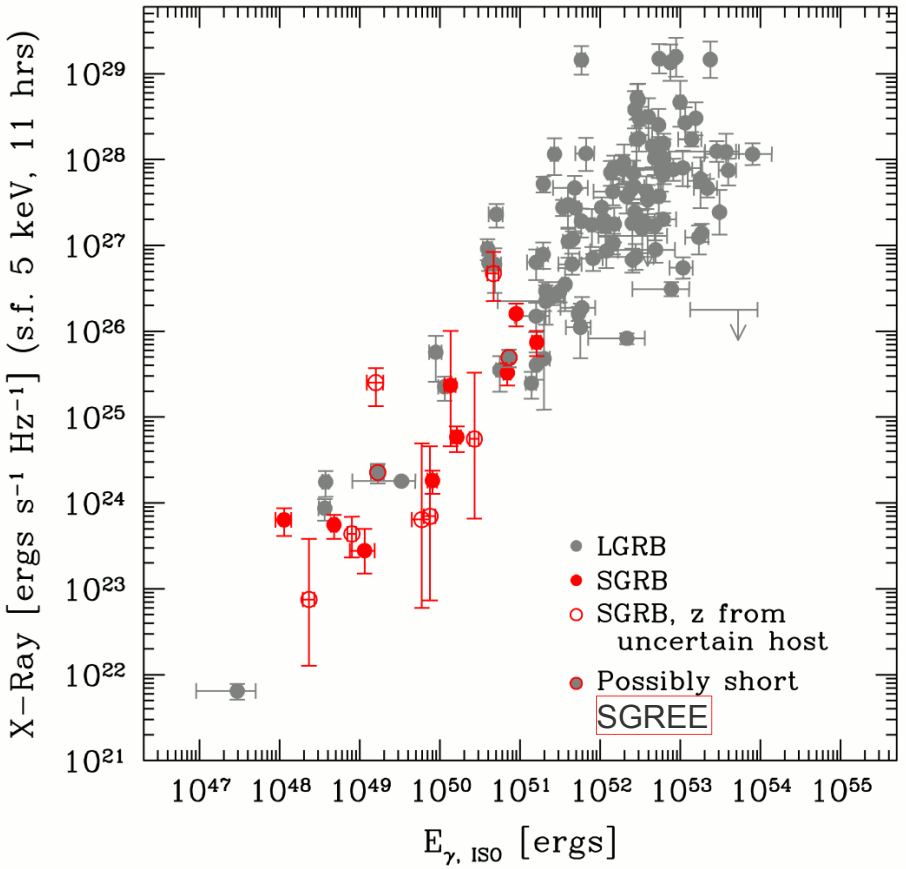

Figure 6. Rest-frame 5 keV X-ray afterglow brightness at 11 hr (rest frame) vs. $E_{\gamma,\mathrm{ISO}}$. The open circles represent SGRBs with a host galaxy determined by XRT error circle only. The classification of GRB 060614 and GRB 060505 is uncertain, therefore they are labeled as "Possibly short."

Nysewander et al. 2009

Short vs Long GRBs

- Brightness and upper limits of SNe measured relative to the peak absolute magnitude of the canonical long GRB-SN 1998bw. SNe associated with long GRBs span a narrow peak brightness range and have a median and standard deviation relative to SN 1998bw of +0.18 ± 0.45 mag. By contrast, the upper limits on SN associations for short GRBs range from 0.6 to 7.4 mag fainter than SN 1998bw. This demonstrates that short and long GRBs do not share a common progenitor system and that at least the short GRBs with deep SN limits are not produced by massive star explosions.

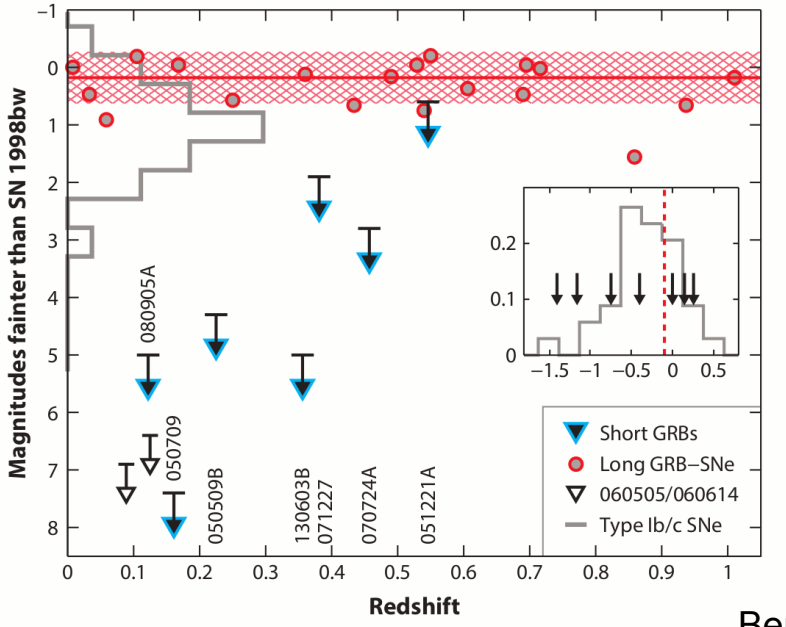

Berger 2014

Figure 2

Limits on supernovae (SNe) associated with short GRBs (*filled triangles*) relative to the peak absolute magnitude of the canonical long GRB-SN 1998bw. Also shown are the distribution of SN peak magnitudes for long GRBs (*filled circles*; *hatched region* marks the median and standard deviation for the population; Hjorth & Bloom 2012), local Type Ib/c SNe (*histogram*; Drout et al. 2011), and two unusual long GRBs that lacked associated SNe (*open triangles*; 060505 and 060614; Della Valle et al. 2006, Fynbo et al. 2006, Gal-Yam et al. 2006, Gehrels et al. 2006). The latter may represent a long duration or extended emission tail of the short GRB population. With the exception of GRB 050509B, all short bursts with limits on associated SNe occurred in star-forming galaxies, indicating that despite the overall star-formation activity, the short GRB progenitors were not massive stars. The inset shows the overall duration distribution of the short GRBs considered in this review (*histogram*); the durations of the 7 short GRBs with SN limits are marked by arrows. The dotted vertical line marks the claimed duration separating *Swift* noncollapsar and collapsar progenitors according to the analysis by Bromberg et al. (2013), and yet three of the short GRBs lacking SN associations have longer durations.

Short vs Long GRBs

- Locations of short GRBs relative to their host centers (offsets). The projected offsets of short GRBs span 0.5–75 kpc with a median of about 5 kpc. These are about four times greater than the median offset for long GRBs.

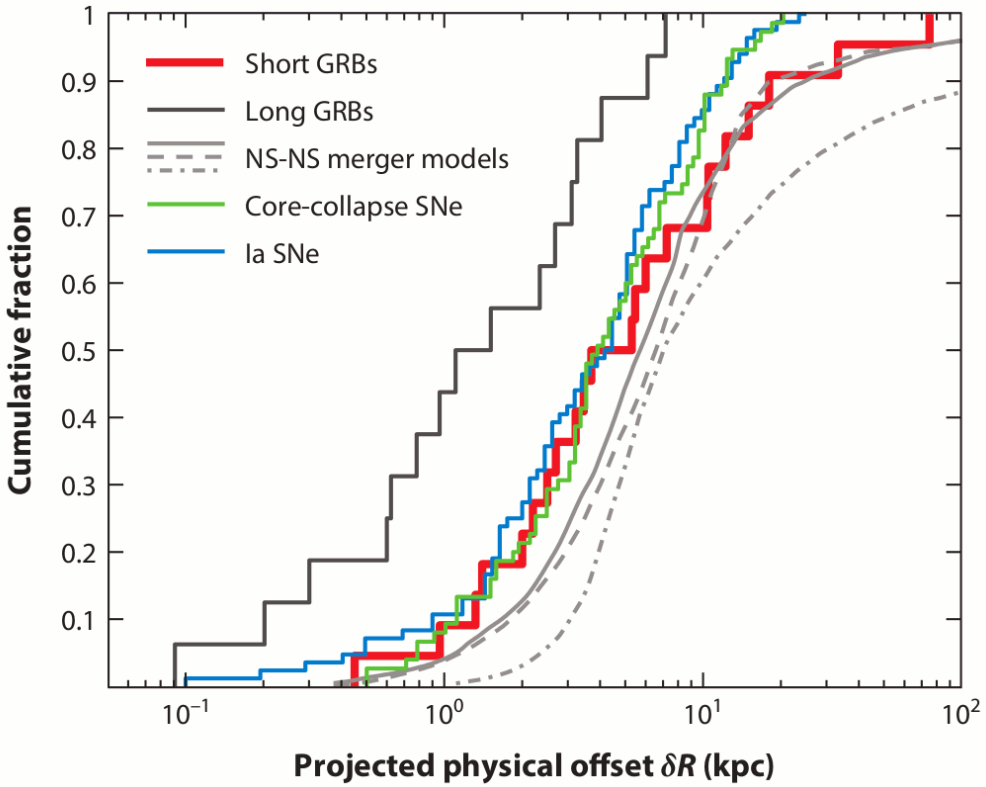

Figure 10 Berger 2014

Cumulative distribution of projected physical offsets for short GRBs with subarcsecond positions (*red*) (Fong, Berger & Fox 2010; Fong & Berger 2013), compared with the distributions for long GRBs (*black*; Bloom, Kulkarni & Djorgovski 2002), core-collapse supernovae (SNe) (*green*; Prieto, Stanek & Beacom 2008), Type Ia SNe (*blue*; Prieto, Stanek & Beacom 2008), and predicted offsets for neutron star (NS) binaries from population synthesis models (*gray*) (Bloom, Sigurdsson & Pols 1999; Fryer, Woosley & Hartmann 1999; Belczynski et al. 2006). Short GRBs have substantially larger offsets than long GRBs and match the predictions for compact object binary mergers. Reprinted from Fong & Berger (2013) with permission.

GRB Prompt Radiation Mechanisms

GRB Prompt Radiation Mechanisms

- Synchrotron emission from a population of relativistic electrons.

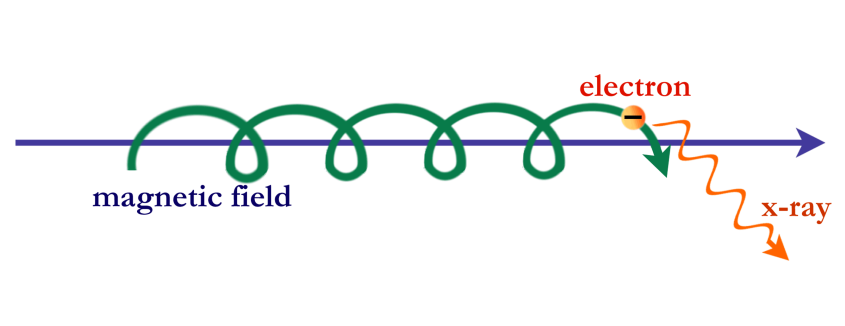

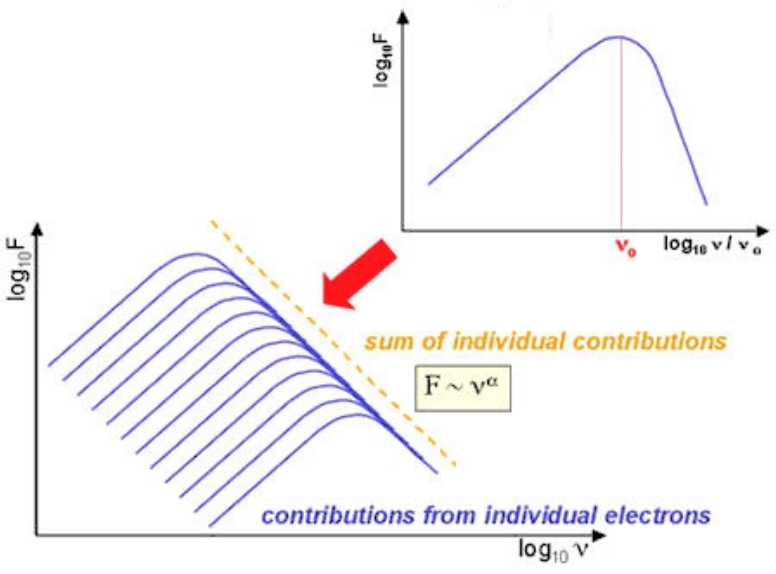

universe-review.ca

GRB Prompt Radiation Mechanisms

- Inverse Compton (IC) scattering of synchrotron photons by relativistic electrons (Synchrotron Self-Compton, SSC model)

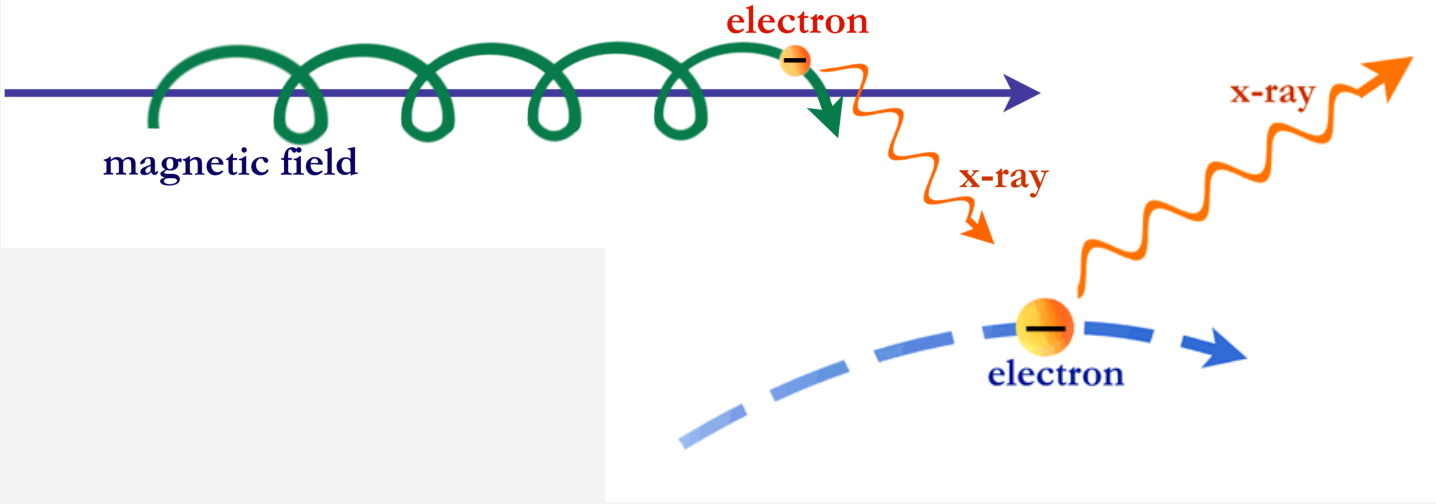

http://chandra.harvard.edu

GRB Prompt Radiation Mechanisms

- Thermal Radiation + Inverse Compton

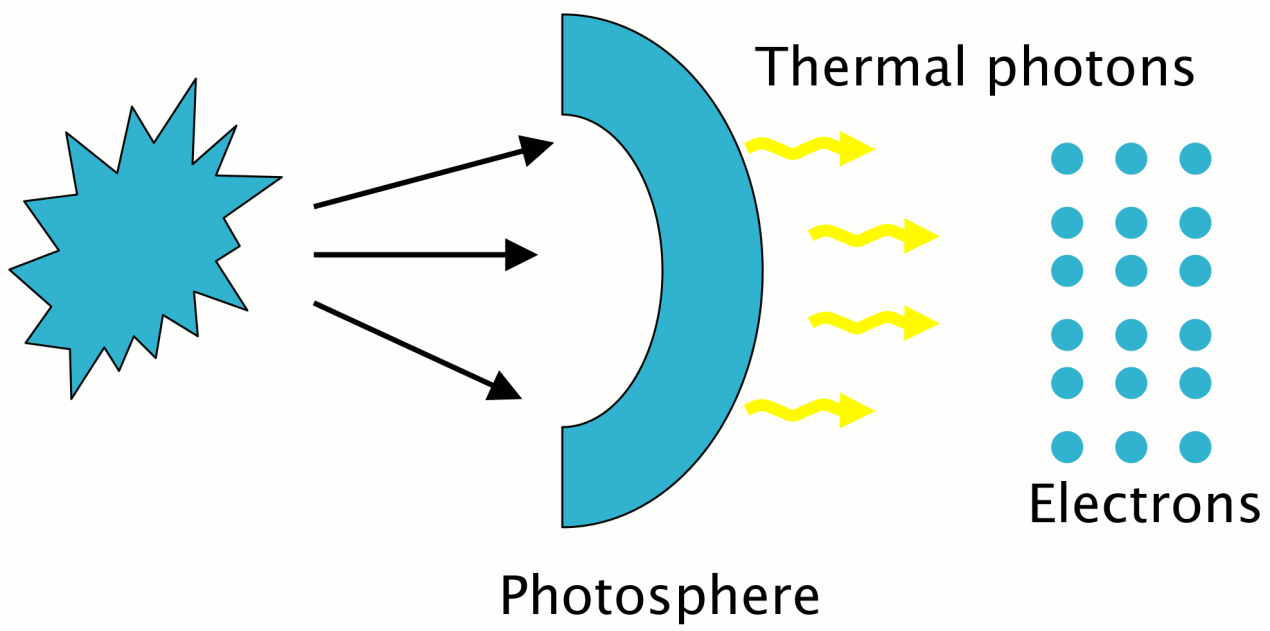

Guidorzi 2010

GRB Prompt Radiation Mechanisms

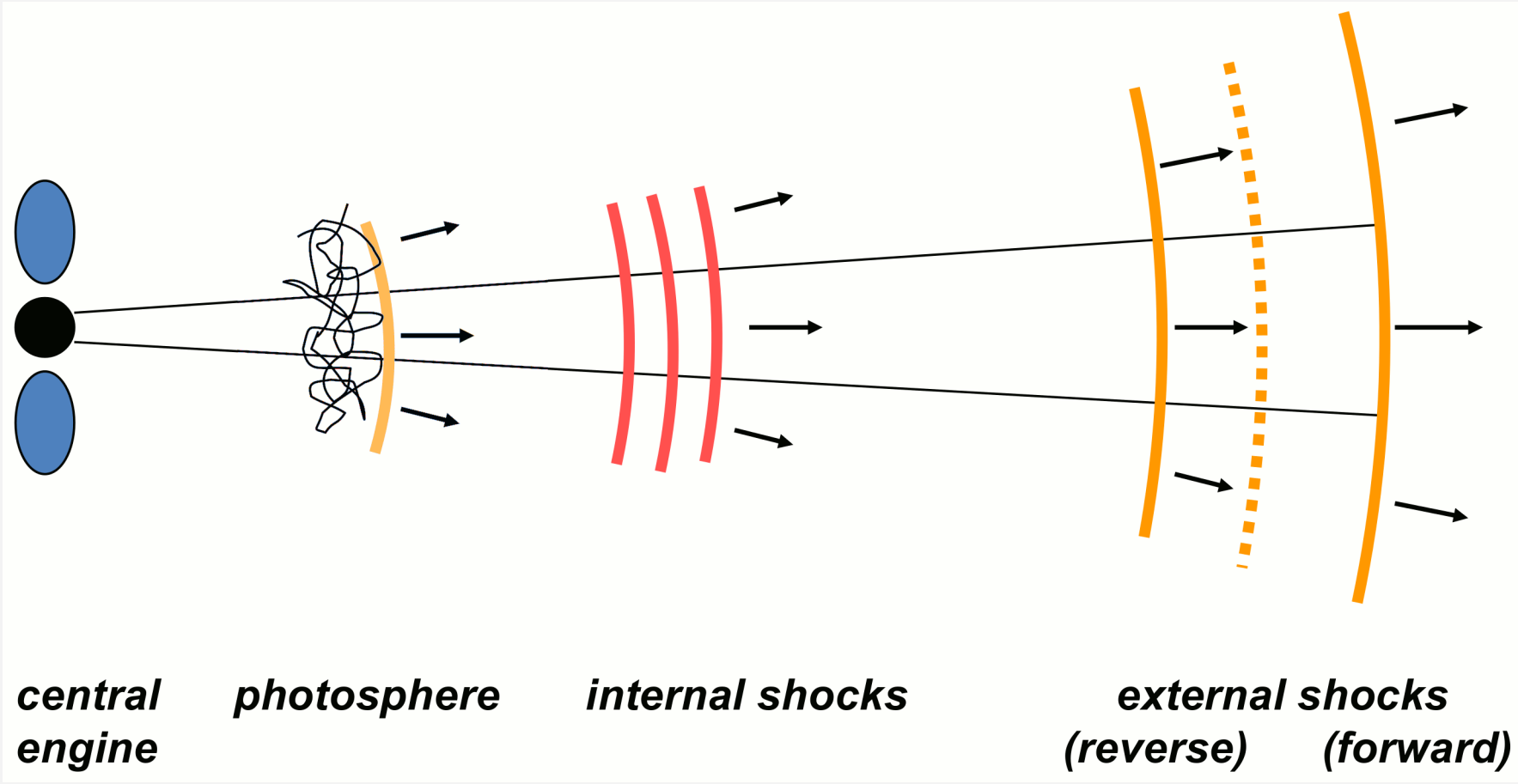

(credit: Bing Zhang)

GRB Prompt Radiation Mechanisms

- Model with a thermal and a nonthermal component (synchrotron emission or Compton radiation). (Ryde 2005) fits prompt emission of some GRBs.
- A strong photospheric emission at gamma-ray wavelengths is predicted in most GRB scenarios, such as in kinetic models (Mészáros & Rees 2000; Daigne & Mochkovitch 2002; Drenkhahn & Spruit 2002; Lyutikov & Usov 2000).

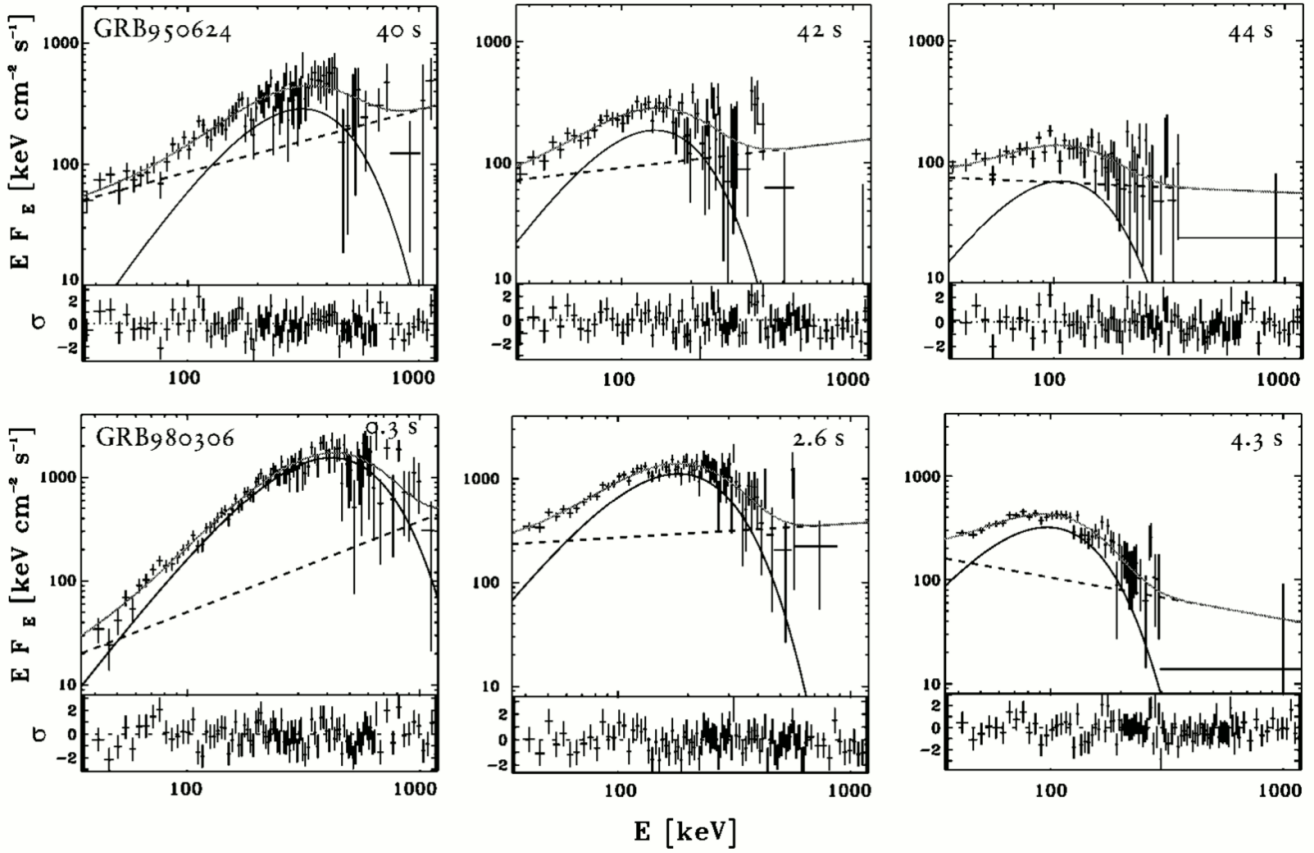

Ryde 2005

FIG. 1.—Hybrid-model spectral fits to *CGRO* BATSE data (~20–1900 keV) for two bursts discussed in the text (GRB 950624, GRB 980306). The time after the trigger of the fitted bin is given in the upper right-hand corner. Note that the investigated pulse in GRB 950624 started at 39.8 s. The nonthermal component is represented by the dashed line, the thermal component by the thick line, and the summed spectrum by the gray line. The spectral data points are rebinned to achieve a signal-to-noise ratio of unity.

GRB Prompt Radiation Mechanisms

- 78% of lGRBs and 85% of sGRBs are incompatible with synchrotron emission (Axelsson et al. 2014).
- 0.3% are pure blackbodies during the whole burst.
- 78% are narrower than the synchrotron function.
- The Planck spectrum can be broaden, but the synchrotron emission cannot be made narrower.

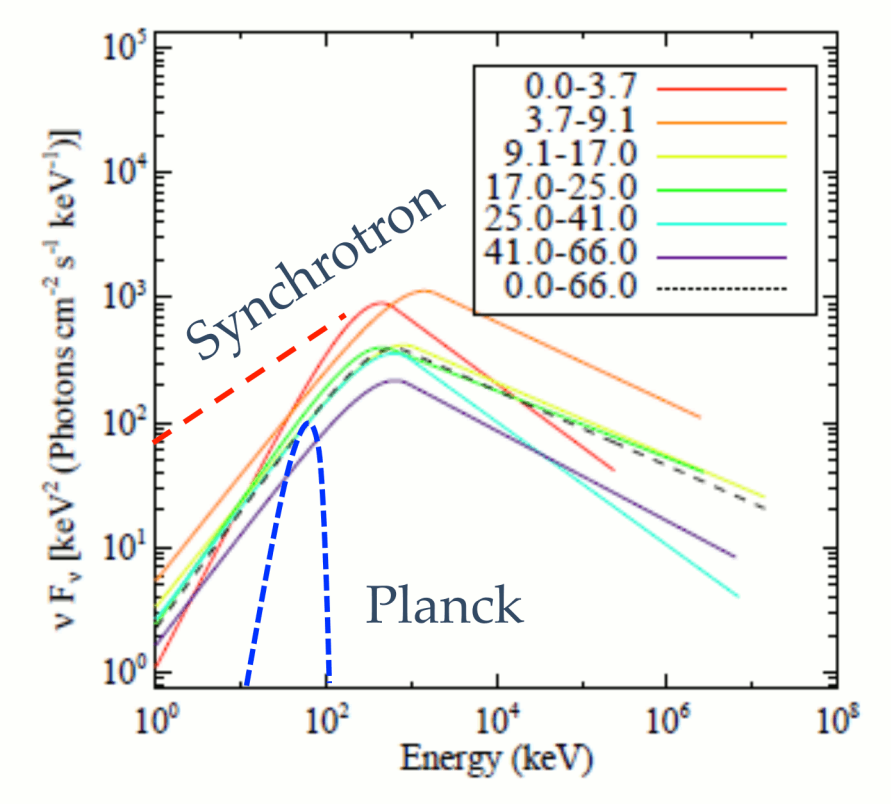

GRB Prompt Radiation Mechanisms

- GRB 090902B, one of the most luminous GRBs prompt emission with Band+PL components and delayed very high energy emission (Abdo et al. 2009).

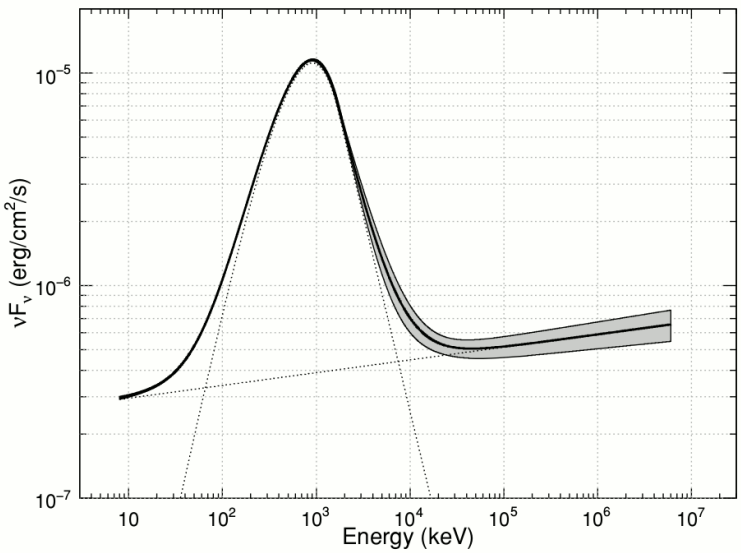

Figure 3. Joint fit of GBM and LAT data to interval **b**, (T_0 +4.6, T_0 +9.6 s). Top: counts spectrum; separate model components are plotted, Band (dashed), power law (solid). Bottom: unfolded νF_ν spectrum. The extension of the >100 MeV power-law component to the lowest energies (<50 keV) is shown.

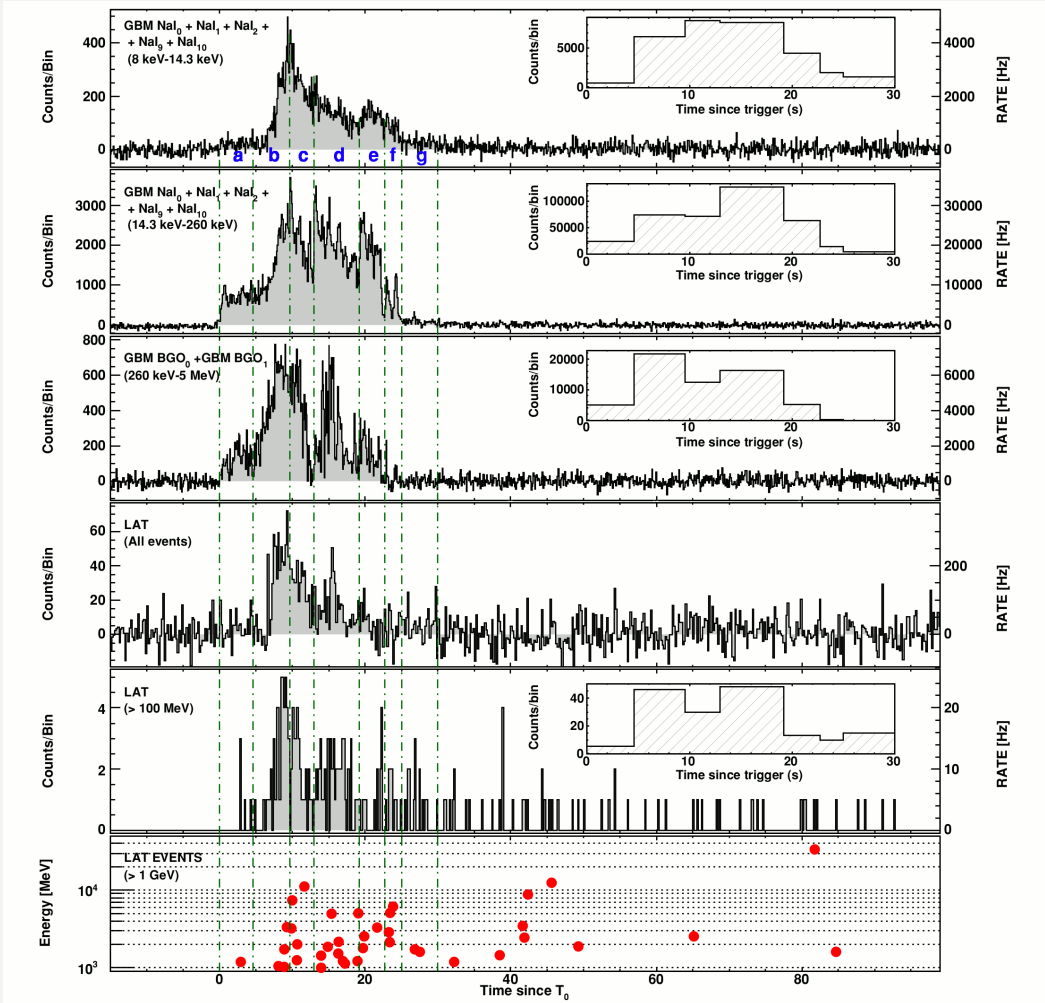

Figure 1. GBM and LAT light curves for the gamma-ray emission of GRB 090902B. The data from the GBM NaI detectors were divided into soft (8–14.3 keV) and hard (14.3–260 keV) bands in order to reveal any obvious similarities between the light curve at the lowest energies and that of the LAT data. The fourth panel shows all LAT events that pass the on-board gamma filter, while the fifth and sixth panels show data for the "transient" class event selection for energies >100 MeV and >1 GeV, respectively. The vertical lines indicate the boundaries of the intervals used for the time-resolved spectral analysis. Those time boundaries are at T_0 + (0, 4.6, 9.6, 13.0, 19.2, 22.7, 25.0, 30.0) s. The insets show the counts for the corresponding data set binned using these intervals in order to illustrate the relative numbers of counts considered in each spectral fit.

GRB Prompt Radiation Mechanisms

- GRB jet composition is diverse
- ”Band” component, thermal component, high energy component

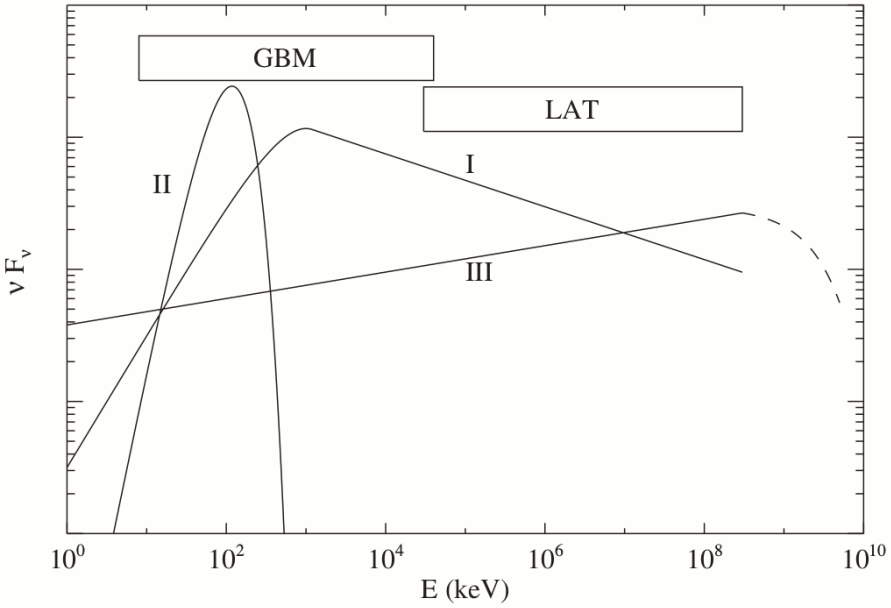

Figure 23. Cartoon picture of three elemental spectral components that shape GRB prompt emission spectra: (I) a Band-function component that is likely of non-thermal origin, (II) a quasi-thermal component, and (III) an extra power-law component that extends to high energies and is expected to have a cutoff near or above the high-energy end of the LAT energy band.

Zhang et al. 2011

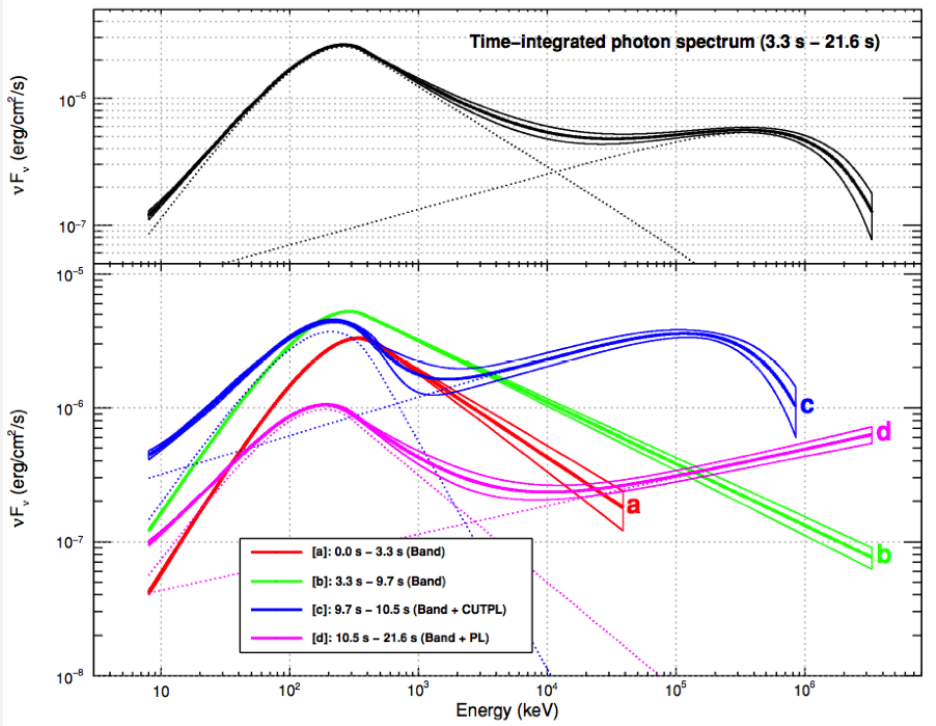

Prompt emission spectra of GRB 090926A at different time intervals (bottom panel) as well as during the entire prompt phase (top panel). A power-law component in addition to the Band spectrum, as also found in other bright LAT-detected GRBs, is required to fit spectra. A cutoff in the PL component at few GeV has been detected in this GRB and in GRB 110731A (Ackermann et al. 2011).

Prompt Gamma-Ray, Prompt Optical and Early Afterglow Polarization

Prompt Gamma-Ray Polarization

- Nature of GRB jets: baryonic or Poynting flux (large-scale magnetic fields)?
- Linear polarimetry can diagnose jet geometry and magnetic field properties within the relativistic jets of GRBs. If prompt GRB *γ*-ray emission is found to be polarized at significant levels, then EM jets are preferred.
- Synchrotron emission → intrinsic polarization
- Coburn & Boggs (2003) claimed linear polarization of 80 ± 20% in prompt gamma-ray emission of GRB 021206 measured by *RHESSI*, but it was disputed by Rutledge & Fox 2004 and Wigger et al. 2003.
- Götz et al. 2005 reported a marginal detection of varying polarization from 4% to 43 ± 25% for GRB 041219A by *INTEGRAL*/IBIS.
- Several other cases reported with *INTEGRAL* and *IKAROS*/GAP:
  i.e. GRB140206A, GRB110301A, GRB100826A, GRB061122, GRB110721A, (Götz et al. 2009; 2013; 2014, McGlynn et al. 2007; 2009, Yonetoku et al. 2011; 2012, Kalemci et al. 2007 etc.).
- Results partly controversial due to calibration issues and fairly low signifcance.

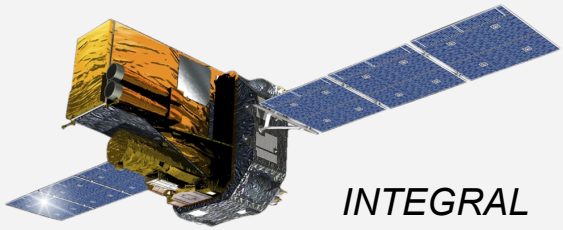

INTEGRAL

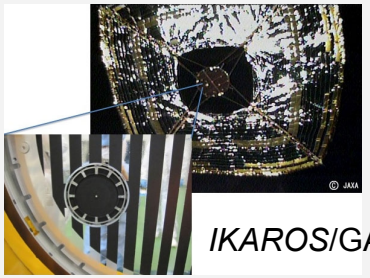

IKAROS/GAP

POLAR

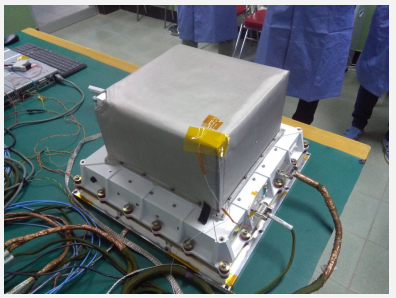

Prompt Gamma-Ray Polarization

GRB	Instr./Sat.	Pol. (%)	Ref.
160530A	COSI	$< 46\%$	[16]
110721A	GAP/IKAROS	84^{+16}_{-28}	[4]
110301A	GAP/IKAROS	70 ± 22	[4]
100826A	GAP/IKAROS	27 ± 11	[3]
021206	RHESSI	80 ± 20	[17]
021206	RHESSI	41^{+57}_{-44}	[18]
140206A	IBIS/INTEGRAL	≥ 48	[19]
061122	IBIS/INTEGRAL	≥ 60	[21]
041219A	IBIS/INTEGRAL	$\leq 4/43 \pm 25$	[20]
041219A	SPI/INTEGRAL	98 ± 33	[15]
960924	BATSE/CGRO	≥ 50	[22]
930131	BATSE/CGRO	≥ 35	[22]

Table 1: List of published GRB polarization measurements

From Kole et al. 2018

- Some key results:
  – high levels (tens of percent) of linear polarization have been seen in some sources
  – variability if timeslicing is possible (usually not)
- Polarization can be due to, e.g., synchrotron radiation in ordered magnetic fields, jet structure, observer's viewing angle, etc. (Götz et al. 2014).

Prompt and Early Optical Emission

- Observations of the early optical emission put constrains to the progenitor models, underlying physical mechanisms, and geometry of the outflow (Gehrels, Ramirez-Ruiz & Fox 2009). UV/optical afterglow comes from external forward shocks.
- The early UV/optical afterglow can be a superposition of emission from the forward shock (FS) and the reverse shock (RS).

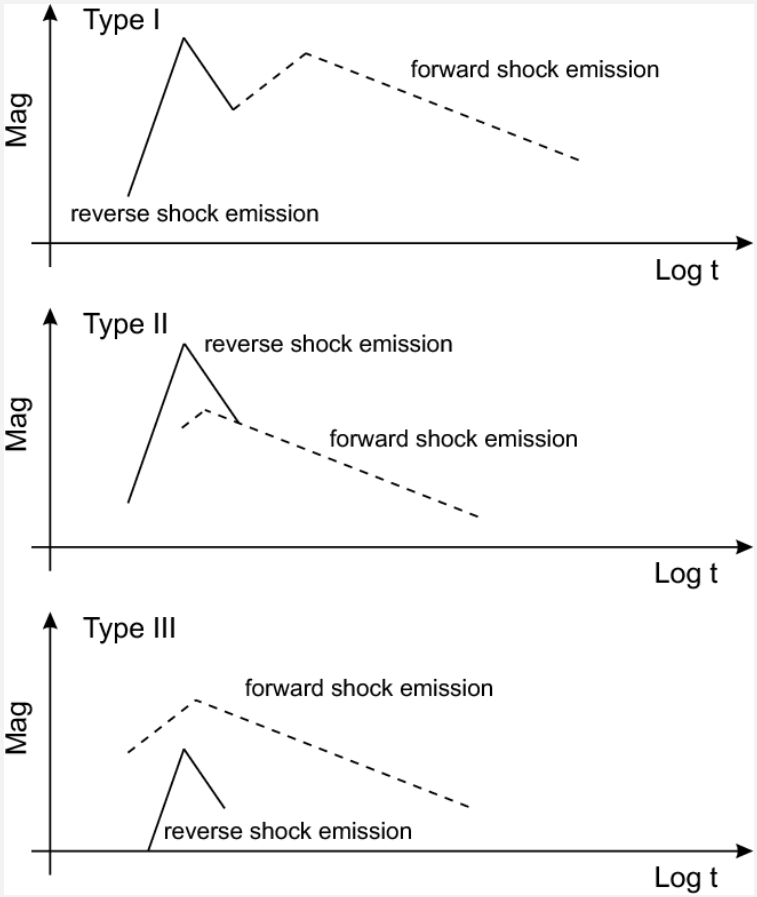

Zhang, Kobayashi, Meszaros 2003; Sari & Piran 1999; Gomboc et al. (2009)

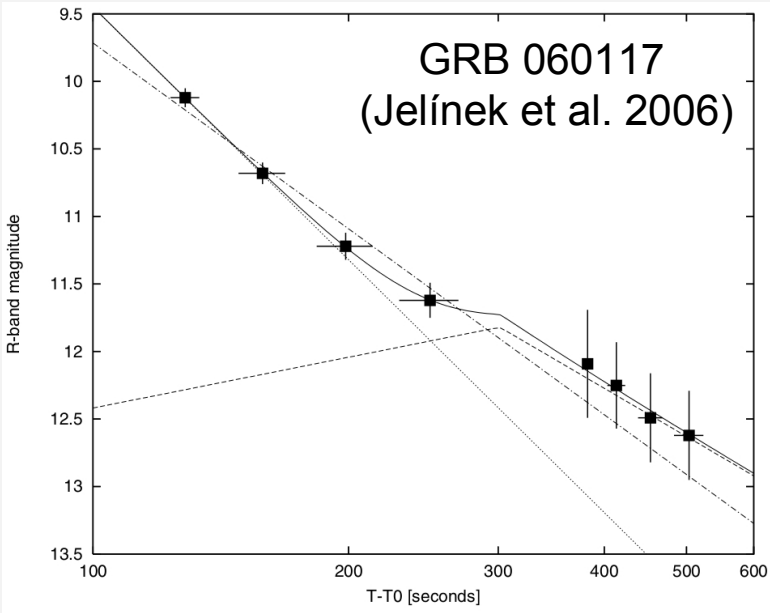

- The detection/non-detection of the RS feature put constrain on the properties of the outflow: magnetized or baryon dominated (Pandey and Zheng 2013).
- In general reverse shock feature is not clearly visible at optical frequencies.
- Strength of RS depends on magnetization content of the ejecta.

Prompt Optical Emission

- Discovery of prompt optical emission of GRB 990123 (Akerlof et al. 1999). Prompt emission is not limited to *γ*-ray domain. Peaked at V = 9 mag !
- Correlation or delay of light curves from different bands gamma and optical needs to be better understood.
- The optical photons sometimes track sometimes don't the *γ*-ray profiles challenging the standard fireball model.
- There are rare measurements of concurrent early optical and gamma emission of only a handful of events since 1999 with usually poor data sampling.
- What about these correlations of early emission of short-duration GRBs?

Vestrand et al. 2005

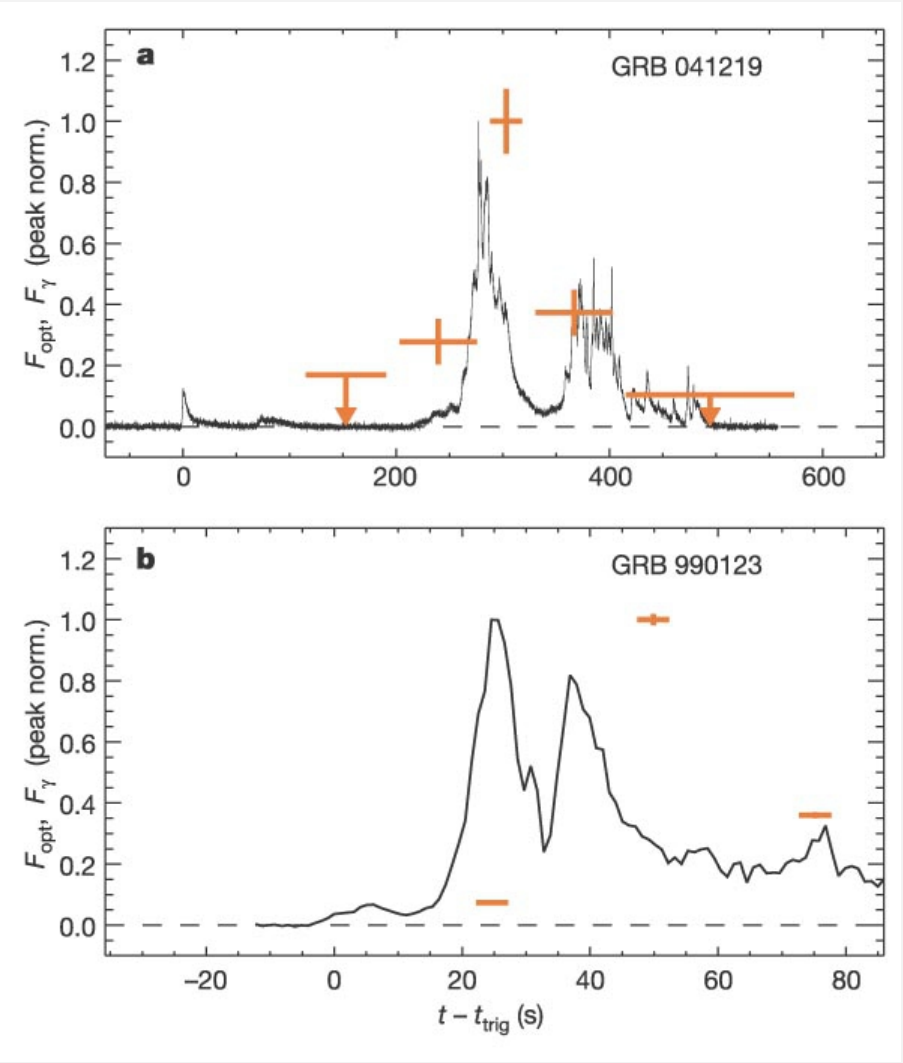

Prompt Optical Emission

Gamma vs optical - ROTSE (Pandey, GRB2012, Marbella)

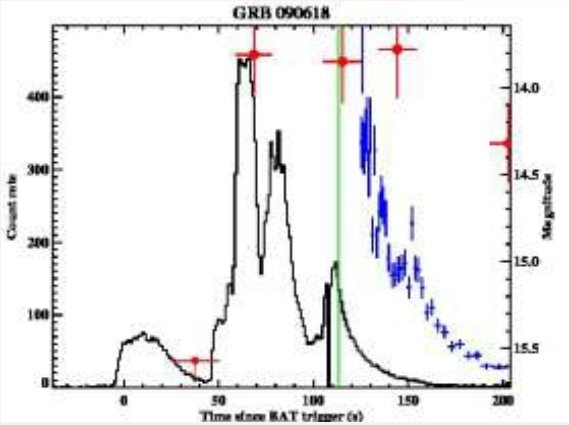

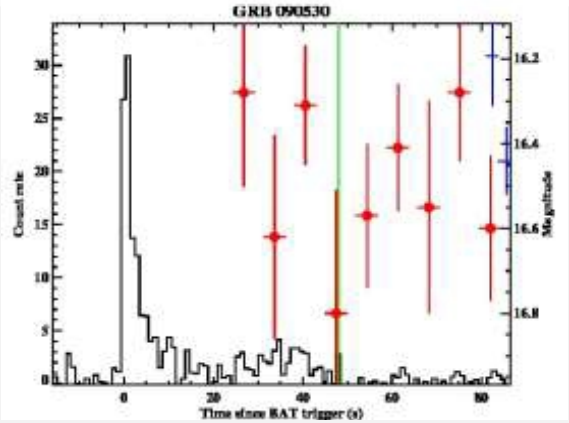

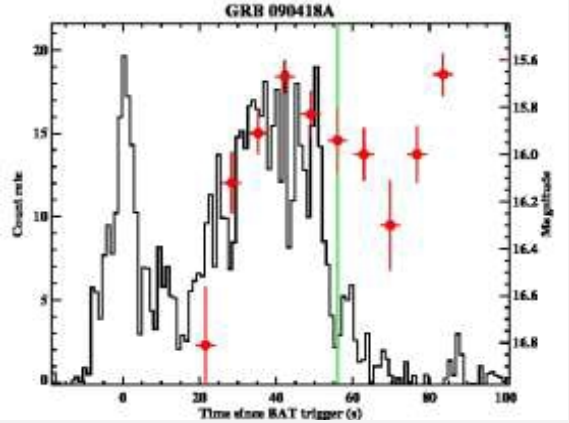

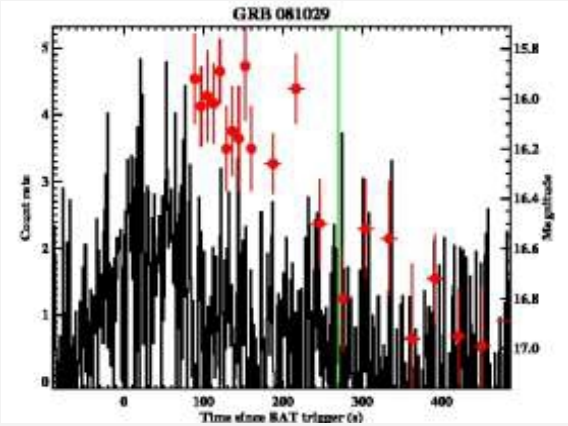

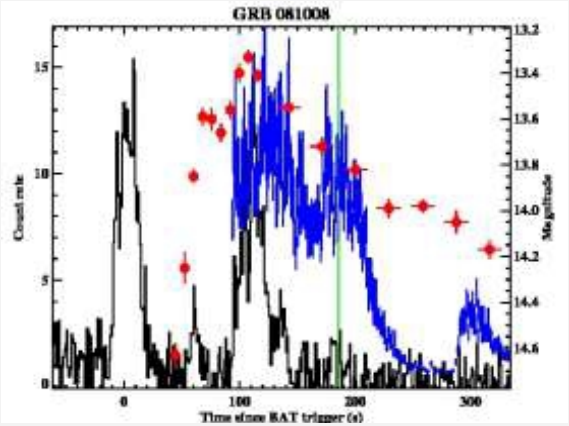

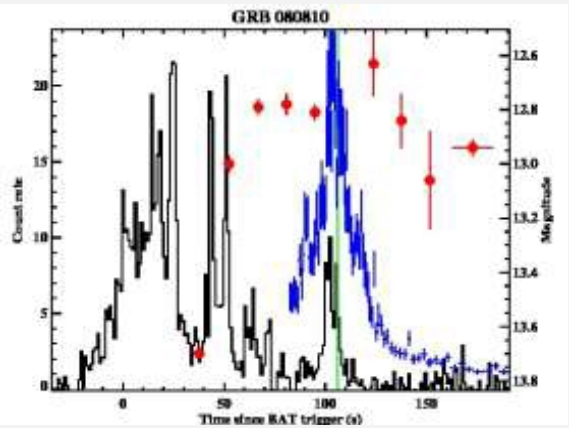

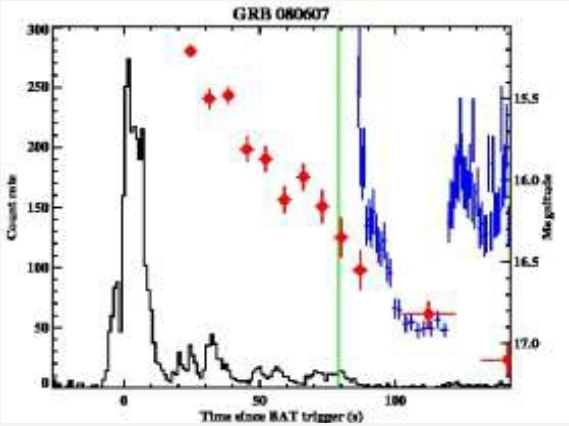

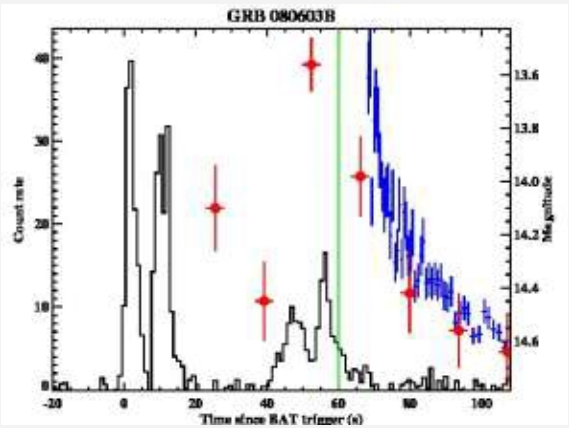

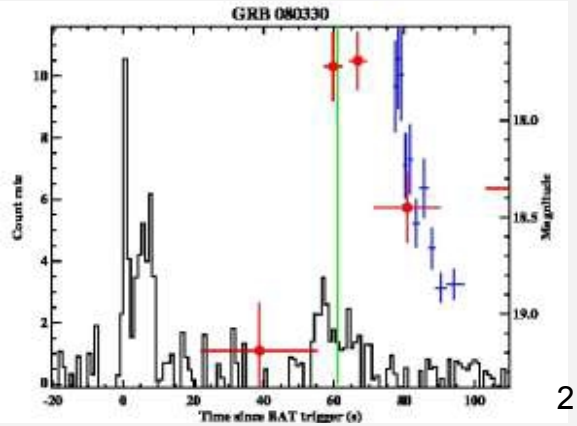

Prompt Optical Emission

First "naked-eye" Burst GRB 080319B

Racusin et al. 2008

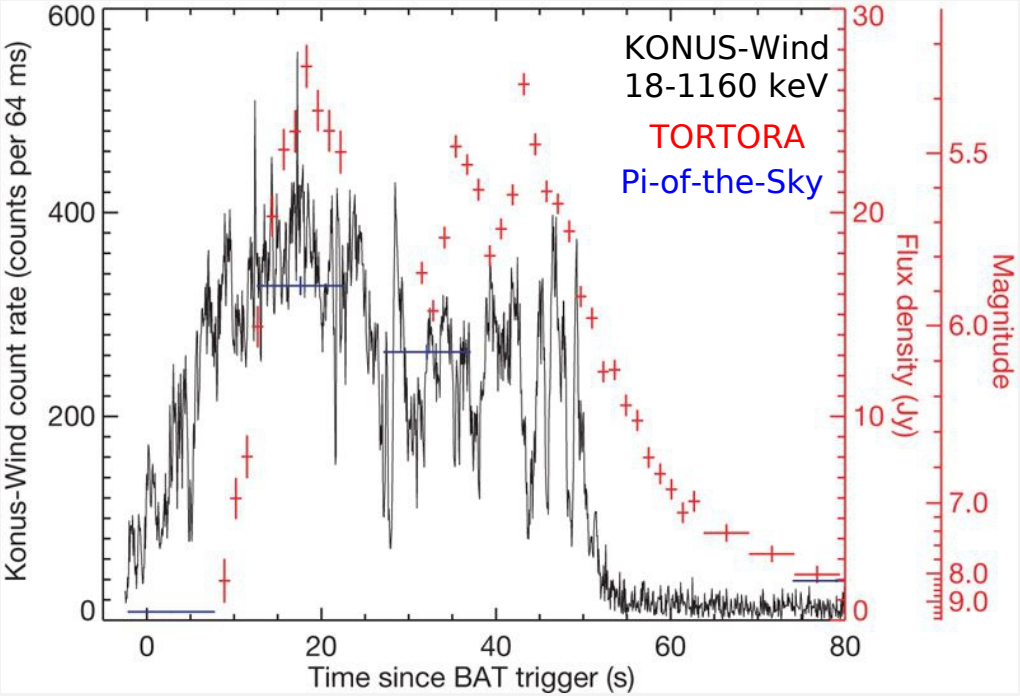

- T_{90} = 50 s
- z = 0.94
- Prompt optical observations:

  Pi-of-the-Sky (Chile)
  RAPTOR (New Mexico)
  REM/TORTORA (Chile)

- Peak brightness of 5.6 magnitudes!!

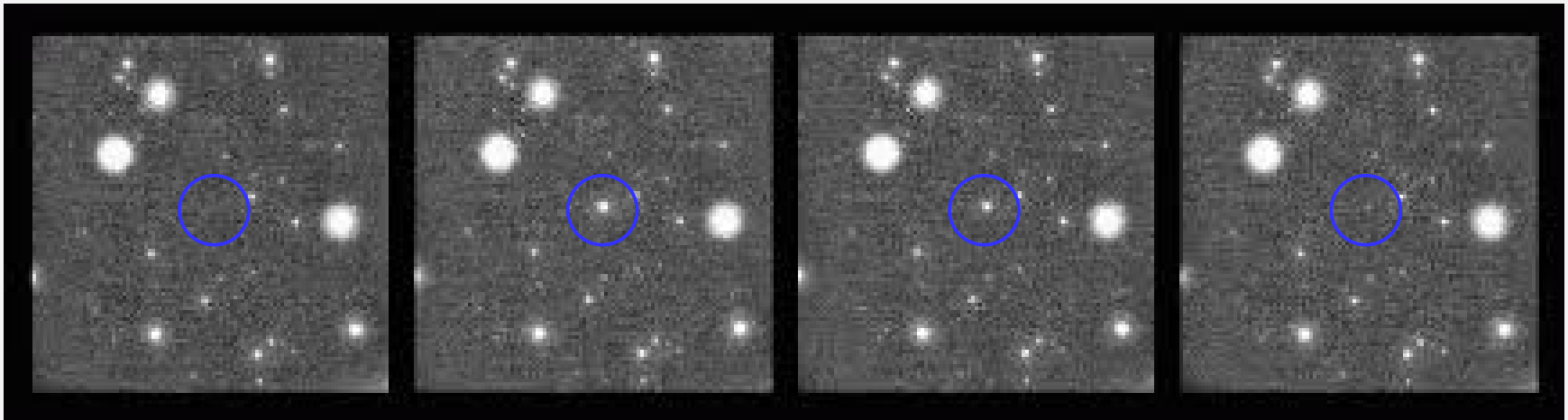

Optical Polarization from Reverse Shock

- Linear polarimetry at optical wavelengths from reverse shock.
- Rev. shocks travel back in ejecta, bright, and may diagnose jet composition.
- High optical linear polarization during reverse shock phase, constant angle, suggests ordered magnetic fields.

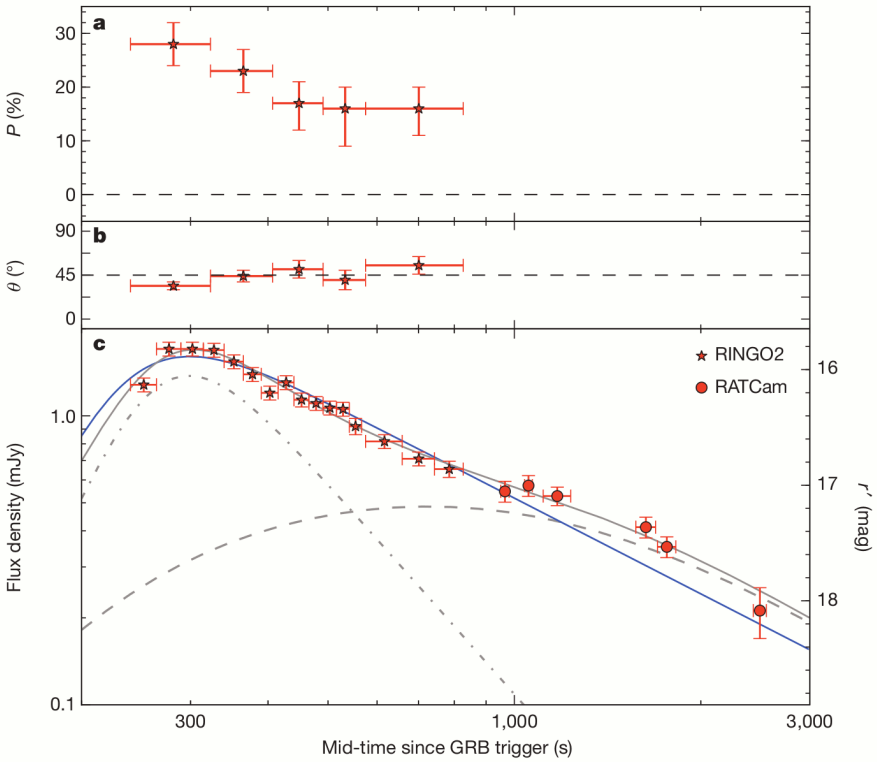

Figure 2 | Evolution of optical polarization and brightness in GRB 120308A. **a**, **b**, Evolution of polarization degree P (**a**) and position angle θ (**b**; degrees east of north) for GRB 120308A. Individual 0.125-s RINGO2 exposures at the eight Polaroid angles are co-added over a desired time interval into eight images, on which absolute aperture photometry is performed and P and θ derived. Owing to the low read noise of the system, data from each rotation angle can be stacked into temporal bins after data acquisition to optimize signal-to-noise ratio versus time resolution. Here the data were subdivided into four bins of duration ~84 s and one bin of ~252 s giving roughly equal signal-to-noise ratio. The observed polarization properties are robust to alternative choices of temporal binning (see Supplementary Information and Extended Data Figs 7, 8, 9). Error bars, $\pm 1\sigma$, as described in Fig. 1b. **c**, Light curve of GRB 120308A in red (555–690 nm) light using RINGO2 and RATCam. Data have been cross-calibrated to the SDSS r' system via five objects in common, with a possible systematic error of up to ~6% between the two instruments due to colour effects. Model fits using one peak (blue solid line) or two peaks (broken grey line for each component; resultant combined light curve in solid grey) are shown with an additional point[26] constraining late time behaviour (see Supplementary Information). The two-peak model is statistically slightly preferred. Error bars, $\pm 1\sigma$.

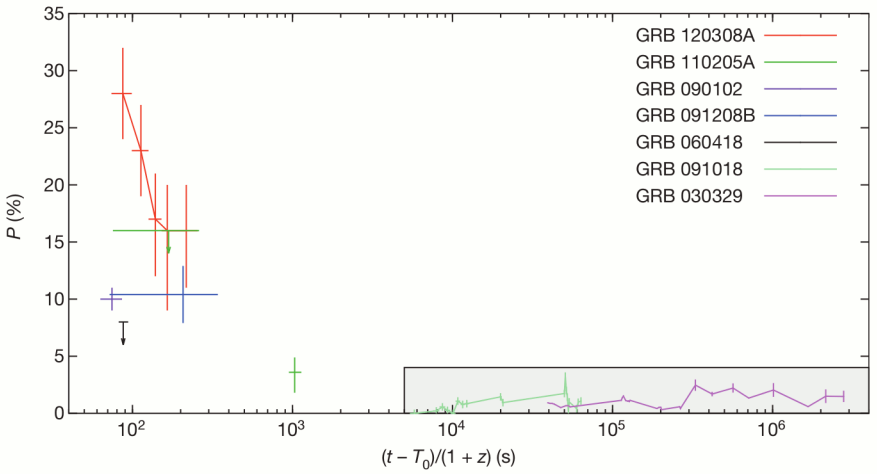

Figure 3 | Rest-frame optical polarization properties of GRBs. The degree of optical polarization P is plotted as a function of time after the burst in the cosmological rest frame, $(t - T_0)/(1 + z)$, where z is redshift and $(t - T_0)$ is the time after the burst in the observer frame. GRB 120308A, GRB 110205A[27], GRB 091208B[6], GRB 090102[8] and GRB 060418[22] were measured at early time. The shaded area shows the typical polarization levels of GRBs measured at late times; representative examples GRB 091018[17] and GRB 030329[16] are shown. Polarization error bars are as reported in the corresponding publications; the temporal error bars show the duration of the measurement. See Supplementary Information and Extended Data Fig. 10 for the determination of redshift for GRB 120308A.

Mundell et al. 2013

Prompt Optical Polarization

- 8.3±0.8% variable linear polarization of a prompt optical flash that accompanied the extremely energetic and long-lived prompt *γ*-ray emission from GRB 160625B.
- Showing that the prompt phase is produced via fast-cooling synchrotron radiation in a large-scale magnetic field that is advected from the black hole and distorted by dissipation processes within the jet (Troja et al. 2017).

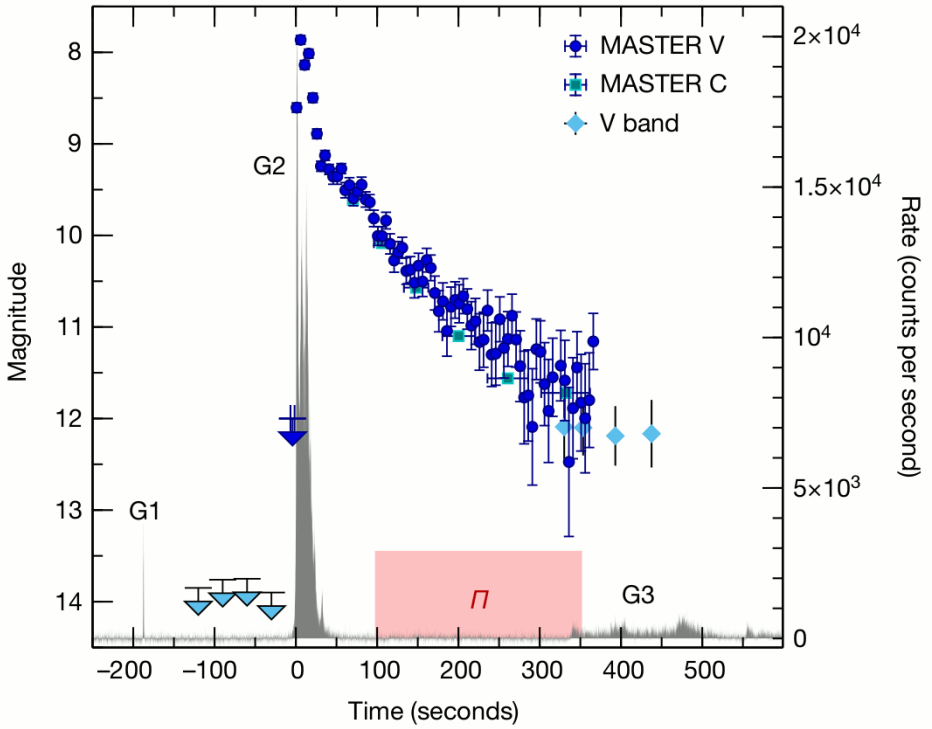

Figure 1 | Prompt γ-ray and optical light curves of GRB 160625B. The γ-ray light curve (black; 10–250 keV) consists of three main episodes: a short precursor (G1), a bright main burst (G2), and a fainter and longer-lasting tail (G3). Optical data from the MASTER Net telescopes and other ground-based facilities[19] are overlaid for comparison. Error bars represent 1σ; upper limits are 3σ. The red box marks the time interval over which polarimetric measurements were taken. Within the sample of nearly 2,000 bursts detected by the GBM, only six other events have a comparable duration (https://heasarc.gsfc.nasa.gov/W3Browse/fermi/fermigbrst.html). Most GRBs end before the start of polarimetric observations.

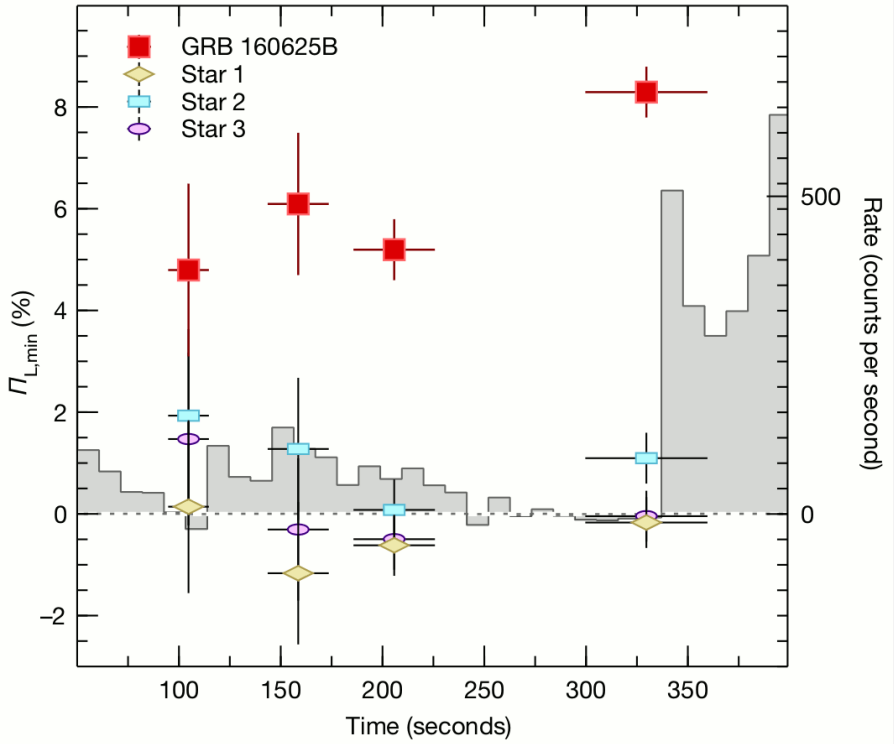

Figure 2 | Temporal evolution of the optical polarization measured for GRB 160625B. The minimum polarization ($\Pi_{L,min}$), measured in four different temporal bins (red squares), remains fairly constant over the first three exposures, then increases by 60% during the fourth (and last) observation. At the same time, an evident increase in the γ-ray count rates (grey shaded area; 5-second time bins) marks the onset of the third episode of prompt emission (G3 in Fig. 1). The spectral shape and fast temporal variability observed during G3 are typical of a GRB's prompt emission. For comparison, we also show simultaneous polarimetric measurements of the three brightest stars in the MASTER-IAC field of view. Error bars represent 1σ.

Dark GRBs and "Orphan" Afterglows

Dark GRBs

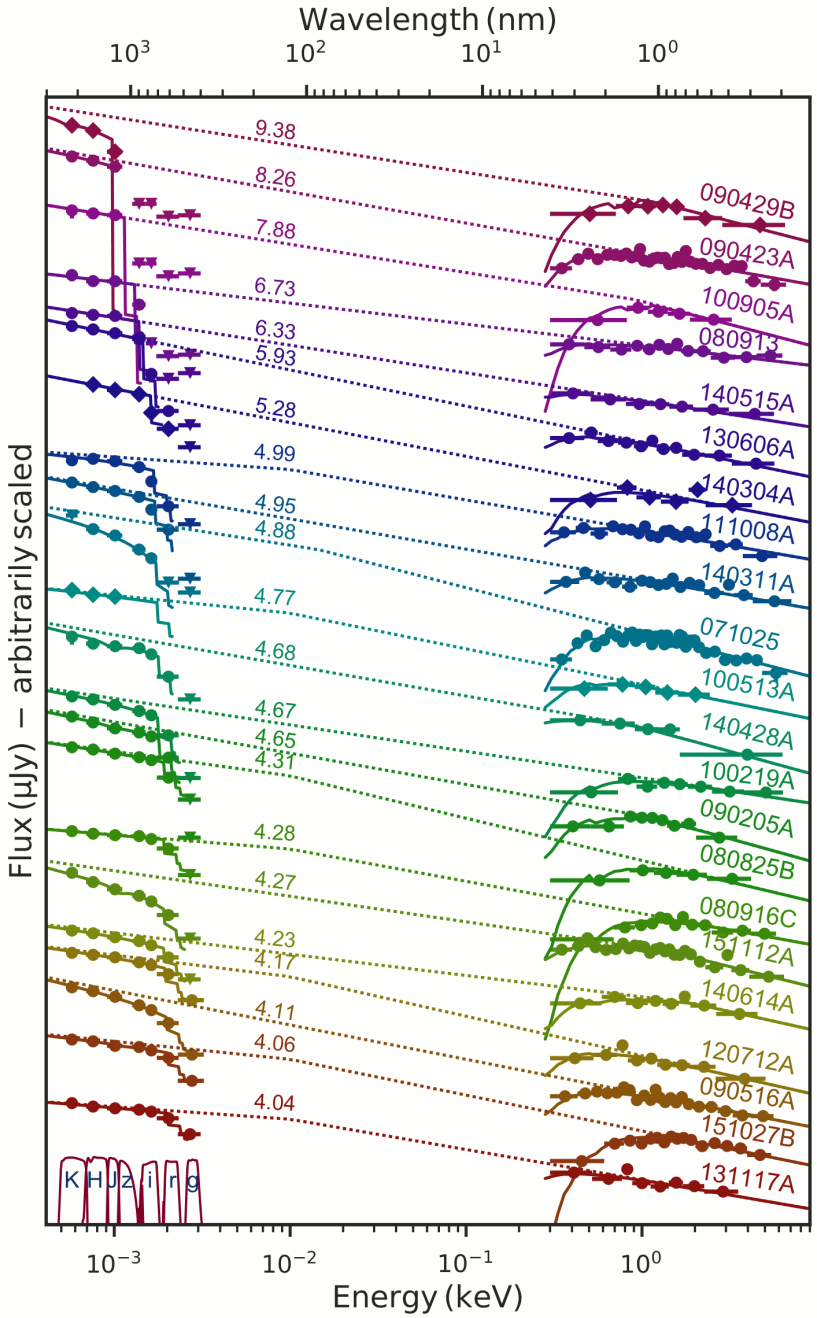

- Various definitions, but usually taken to mean a long-GRB for which the optical afterglow is sub-luminous compared to the X-ray afterglow.
- With the advent of Swift:
  - 25-35% LGRBs are dark (with dusty environment, very few at high *z*)
  - lack of optical flashes
- In most cases the GRB is dark due to a significant absorption of the optical radiation in the medium of the host galaxy.

Bolmer et al. 2018

Fig. 7. Spectral energy distribution for the 22 GRBs analyzed in this paper with increasing redshift from the bottom to top (as labeled). Data for GRBs detected with GROND are plotted with circles, data from other instruments with diamonds. The X-ray spectrum, if not available simultaneously to the optical and NIR data, was flux normalized to the mid-time of the chosen GROND exposure. Dashed lines indicate the unabsorbed best-fit models. Solid lines indicate the best-fit model including absorption: in the X-rays due to galactic plus host intrinsic absorption by medium weight metals; in the optical and NIR range due to host intrinsic absorption by dust (the data were corrected for galactic foreground reddening beforehand). The flux on the *y*-axis is completely arbitrary to get a better visualization. In the left corner at the bottom of the plot we also show the GROND filter curves.

Off-axis "Orphan" Afterglow

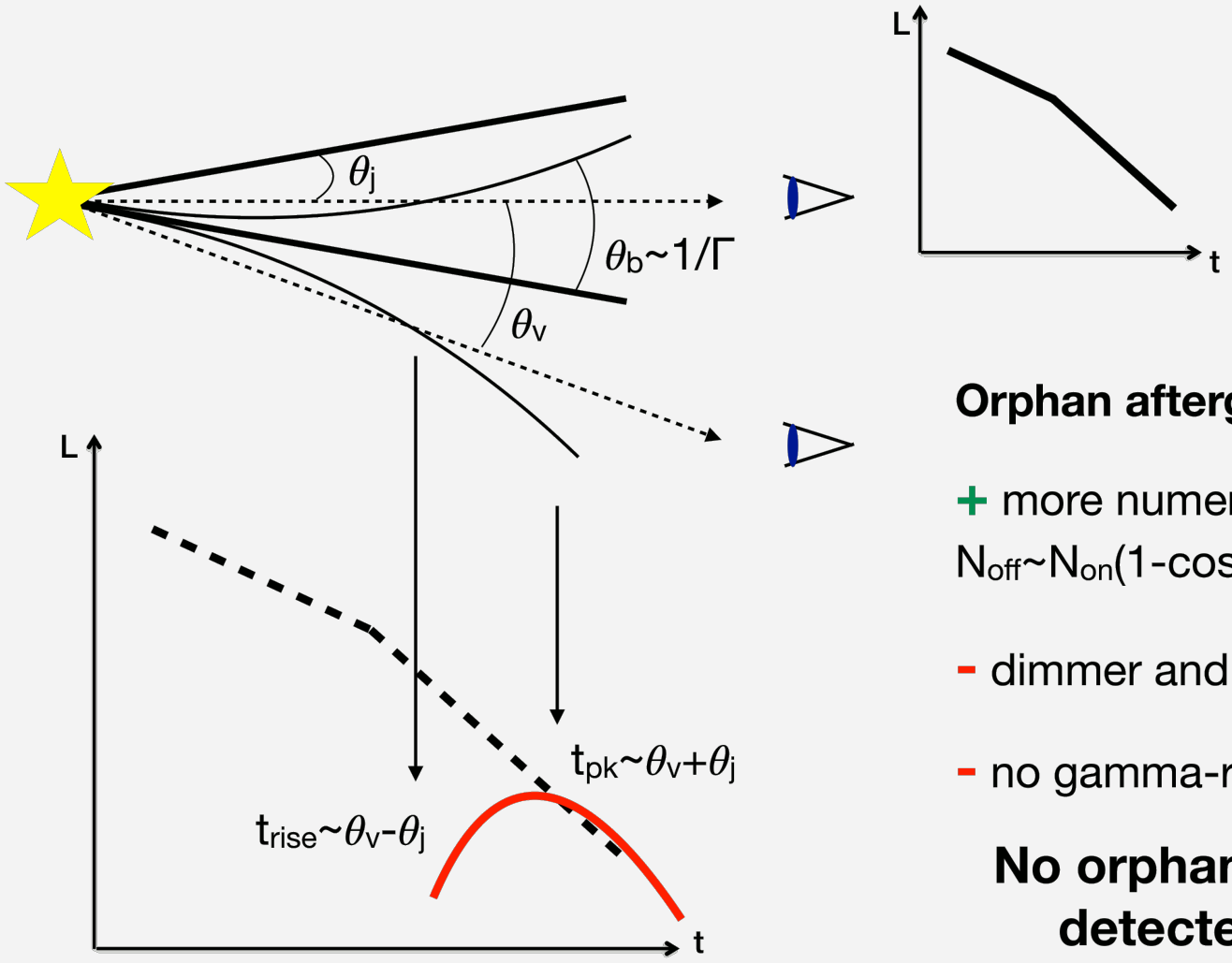

Orphan afterglows:

+ more numerous,
$N_{off} \sim N_{on}(1-\cos\theta_j)^{-1} \sim 200\ N_{on}$

- dimmer and delayed

- no gamma-ray trigger

No orphan afterglow detected so far

- Most of the past surveys had small chances to detect OAs. Better prospects for new and future surveys:
- In optical: ~2 OT/yr with Gaia, ~20 OA/yr with Zwicky Transient Facility (ZTF), ~50 OA/yr with Large Synoptic Survey Telescope (LSST)
- In X-rays: ~30 OA/yr with eROSITA (Ghirlanda et al. 2015)

Other Possible “Types” of GRBs: Short GRBs with Extended Emission, X-Ray Flashes, Low-Luminosity GRBs, Ultra-long GRBs

Various Bursts and Not Only GRBs

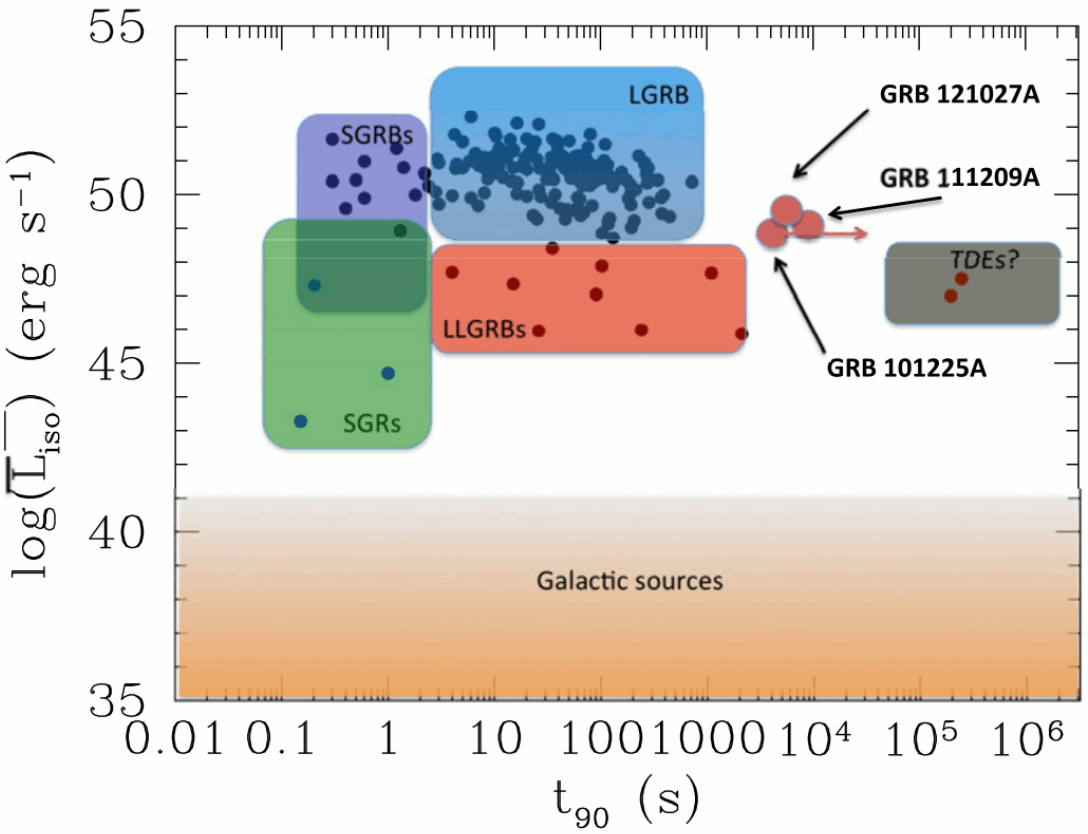

Figure 2. Parameter space for transients in the γ-ray sky, showing the duration of the burst and the approximate average luminosity over that duration. At low luminosity, there are numerous Galactic sources that we do not include in further detail; at higher luminosity, the outbursts for soft-gamma repeaters (SGRs) in our own Galaxy are shown, as well as extragalactic transients such as long- and short-duration GRBs (LGRBs and SGRBs) and the likely population of low-luminosity GRBs (LLGRBs). Two recently discovered very long transients, thought to be from TDEs, are also shown. The bursts considered in this paper (GRB 101225A, GRB 111209A, and GRB 121027A) are clearly outliers in any of these aforementioned classes.

Levan et al. 2014

Short GRBs with Extended Emission (SGRBEE)

- Nearby (z = 0.125) GRB 060614 does not fit into either SGRB or LGRB class. Its 102-s duration groups it with long-duration GRBs, while its temporal lag and peak luminosity fall entirely within the short-duration GRB subclass. Very deep optical observations exclude an accompanying supernova.

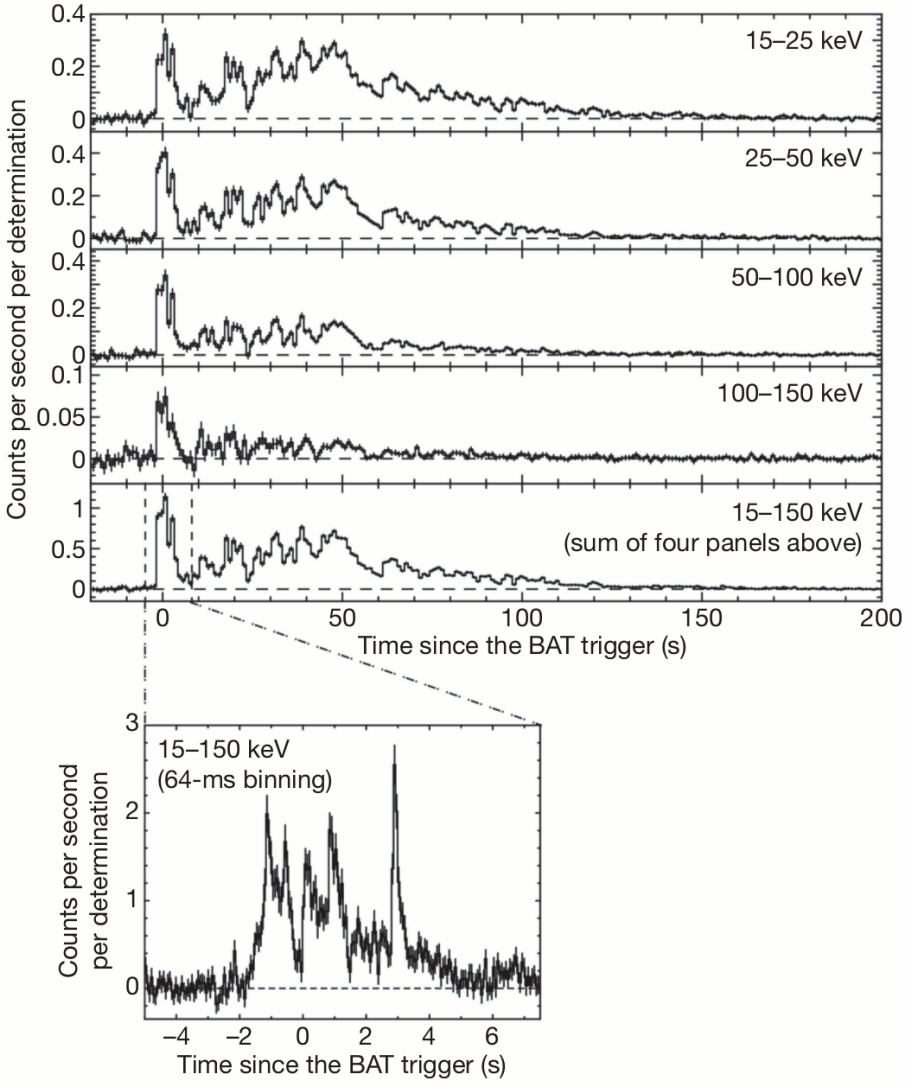

Figure 1 | The light curve of GRB 060614 as observed with the BAT.

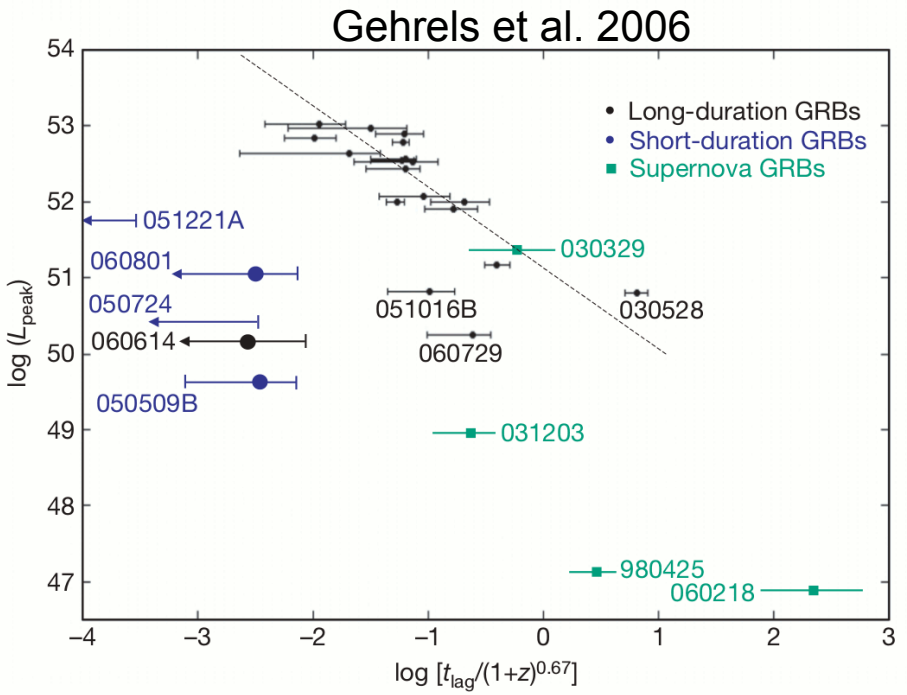

Figure 2 | Spectral lag as a function of peak luminosity showing GRB 060614 in the region of short-duration GRBs.

- Another case of long nearby GRB without SN: GRB 060505 at z = 0.089
- Accretion-induced collapse in binary system; white dwarf-white dwarf mergers; star collapse without enough ^{56}Ni, etc... ?

Short GRBs with Extended Emission (SGRBEE)

- One class of apparently short duration bursts is characterized by a long “tail” of soft X-ray emission. T_{90} can formally therefore be long.
- Not associated with core-collapse SN like LGRBs.

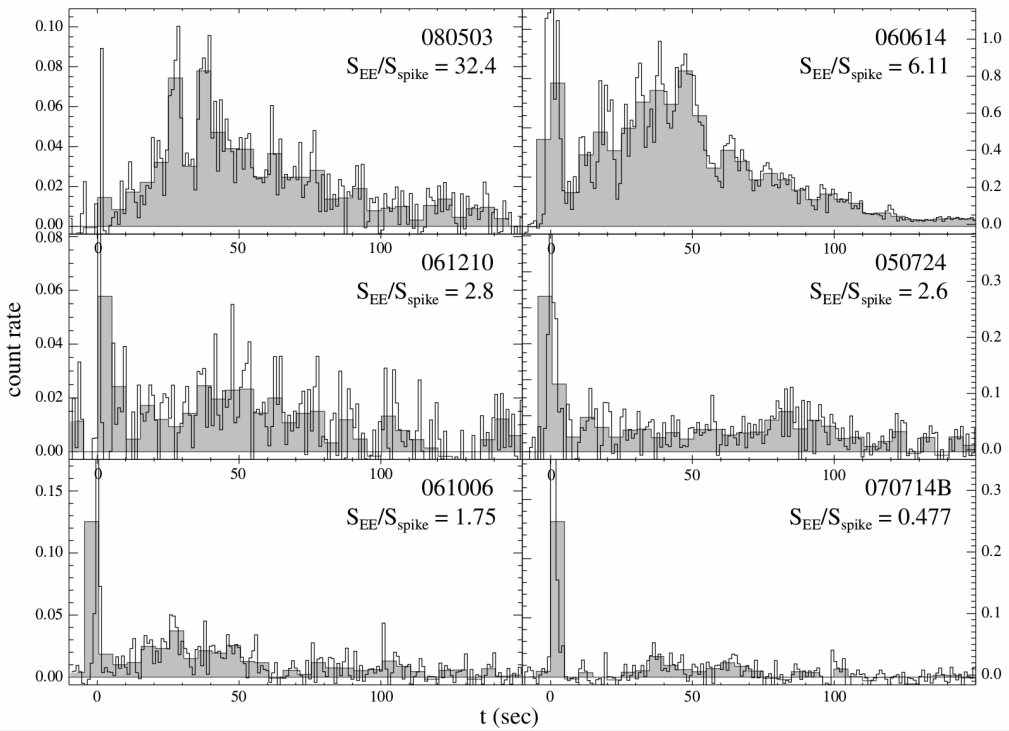

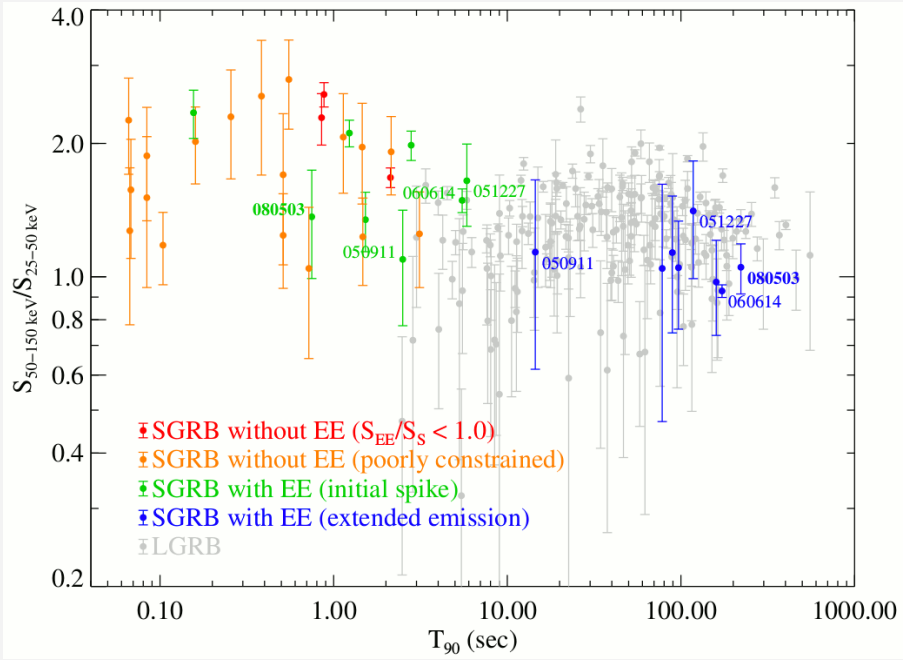

Perley et al. 2009

- See also Norris and Bonnell 2006 with GRBEE in BATSE data.

Short GRBs with Extended Emission (SGRBEE)

- Offsets from hosts of SGRBEE seem to be less than the for SGRB without extended emission and similar to those of LGRB.

SHBs without EE

Median offset 22 kpc

Spread $\sigma \sim 26$ kpc

SHBs + EE

Median offset 2.5 kpc

Spread $\sigma \sim 3.4$ kpc

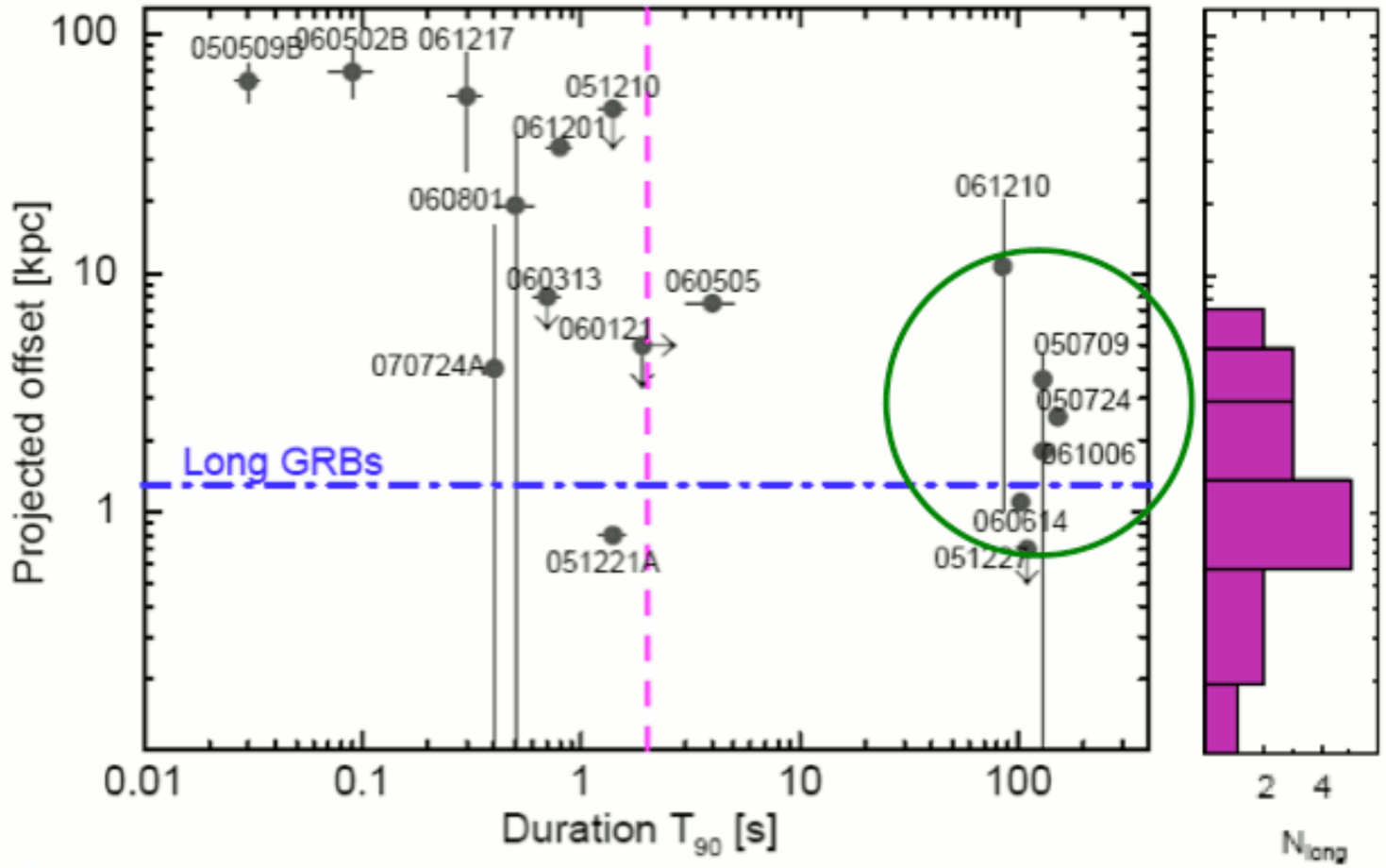

LGRBs from Bloom+02

Slide from E. Troja, Santa Fe: GRBs 2007

X-Ray Flashes

- Seem to be long-duration GRBs with unusually soft spectra.
- Some accompanied by SNe.
- Possible explanations for spectral properties: high-redshift? off-axis? low differential velocities? low velocity jet?
- Events described as:
  X-Ray Rich GRBs (XRRs) if $\log[S_X(2\text{-}30\ \text{keV}) / S_X\ (30\text{-}400\ \text{keV})] > -0.5$ and
  X-Ray Flashes (XRFs) if $\log[S_X(2\text{-}30\ \text{keV}) / S_X(30\text{-}400\ \text{keV}) > 0$

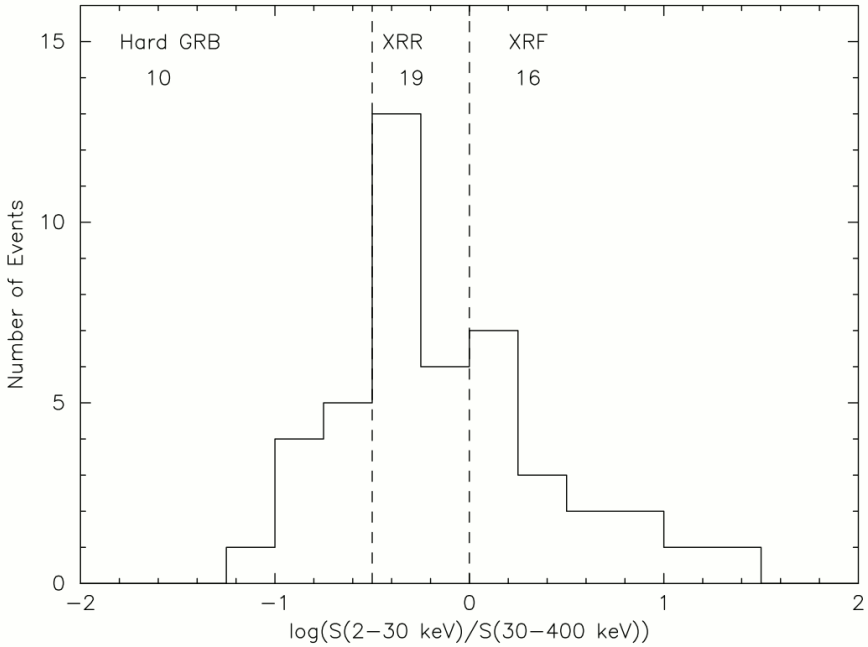

FIG. 2.—Distribution of the fluence ratio $S_E(2-30\ \text{keV})/S_E(30-400\ \text{keV})$. The dashed lines correspond to the borders between hard GRBs and XRRs, and between XRRs and XRFs.

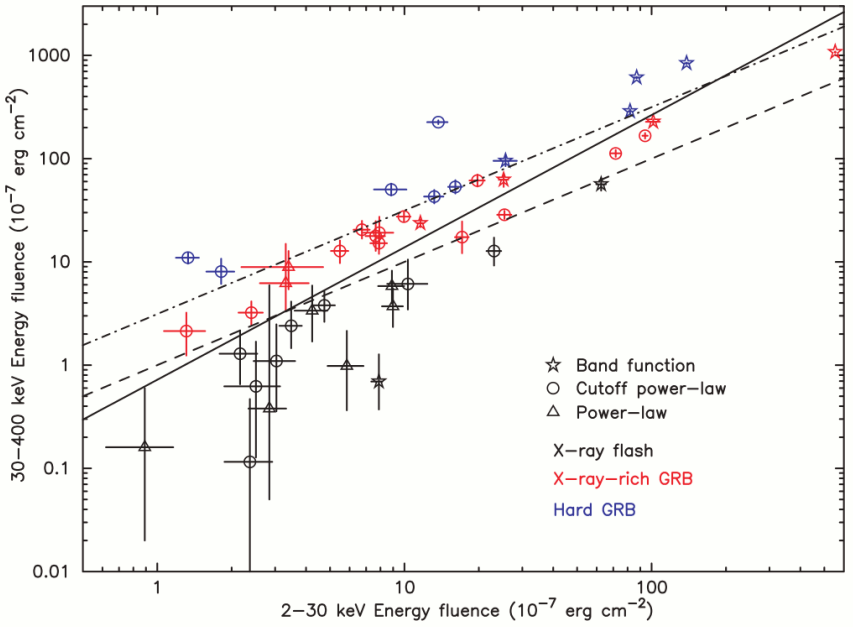

FIG. 3.—Distribution of the bursts in this study in the $[S_E(2-30\ \text{keV}), S_E(30-400\ \text{keV})]$ plane. The dashed line corresponds to the boundary between XRFs and XRRs. The dot-dashed line corresponds to the boundary between XRRs and GRBs. The solid line is the best linear fit to the burst distribution and is given by $S_E(30-400\ \text{keV}) = (0.722 \pm 0.161) \times S_E(2-30\ \text{keV})^{1.282 \pm 0.082}$. The correlation coefficient of the burst distribution is 0.851. The probability of such a correlation occurring by chance for the sample size of 45 bursts is 1.1×10^{-8}.

Sakamoto et al. 2005

Low-Luminosity GRBs

- Low luminosity 10^{46}-10^{48} erg/s (~10^{-4} than long GRBs), E_{iso}=10^{48}-10^{50} erg

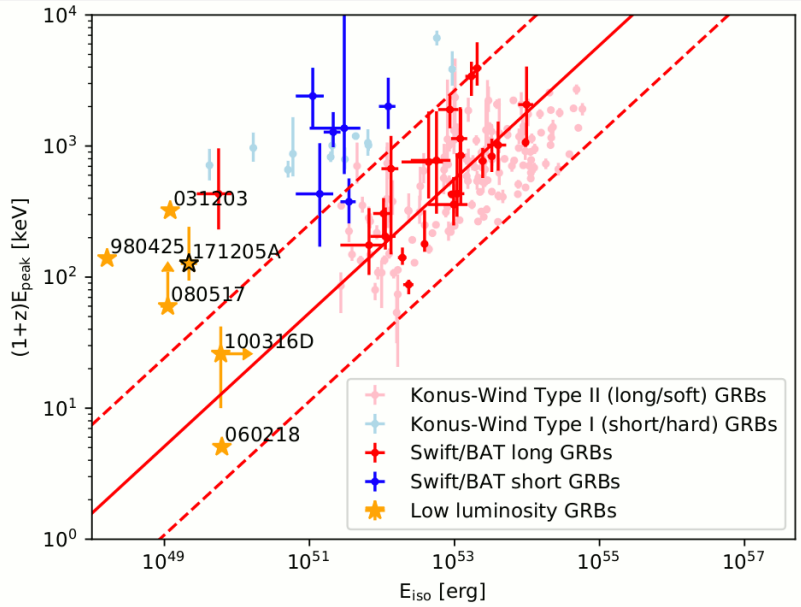

Fig. 9. E_{peak} in rest-frame versus E_{iso}. The *Swift*/BAT GRB sample (dark blue and red) is adapted from Krimm et al. (2009). The Konus-*Wind* GRB sample (light blue and red) is adapted from Tsvetkova et al. (2017). The yellow stars show GRB 171205A and several sources defined as low-luminosity GRBs in previous studies (Campana et al. 2006; Ghisellini et al. 2006; Starling et al. 2011; Stanway et al. 2015). The red lines are the best fit (solid line) and the 2.5σ variation (dashed line) reported in Krimm et al. (2009).

D'Elia et al. 2018

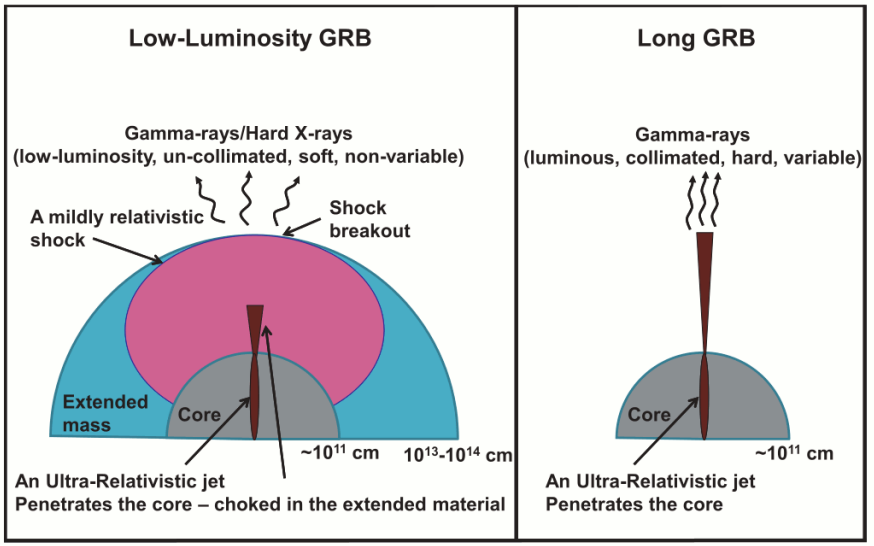

Figure 2. Schematic sketch illustrating the similarity and differences between *ll*GRBs and LGRBs. Both explosions go through a collapse of a similar core which leads to the formation of a similar GRB engine and to a similar SN explosion. In both types the GRB engine launches ultra-relativistic narrowly collimated jet, which penetrates through the core. In LGRBs the jet is free to expand as soon as it is out of the core where it produces a luminous, hard, narrowly collimated beam of gamma rays which can vary in time on short timescales. In *ll*GRB the jet emerges from the core into the low-mass extended material where it is choked and any radiation that it produces is absorbed and cannot reach to the observer. The jet energy is deposited in the extended material driving a strong shock into it. The shock is much less relativistic than the jet (most likely Newtonian) and it accelerates before breakout (often to a mildly relativistic velocity). Upon breakout it produces low-luminosity soft gamma rays which show no significant variability with time and are not narrowly beamed.

Nakar 2015

Ultra-Long GRBs

- Lasting >1-10 ks
- e.g. GRB 101225A, GRB 111209A, GRB 121027A, GRB 130925A
- Proposed to form a separate class, caused by the collapse of a blue supergiant.

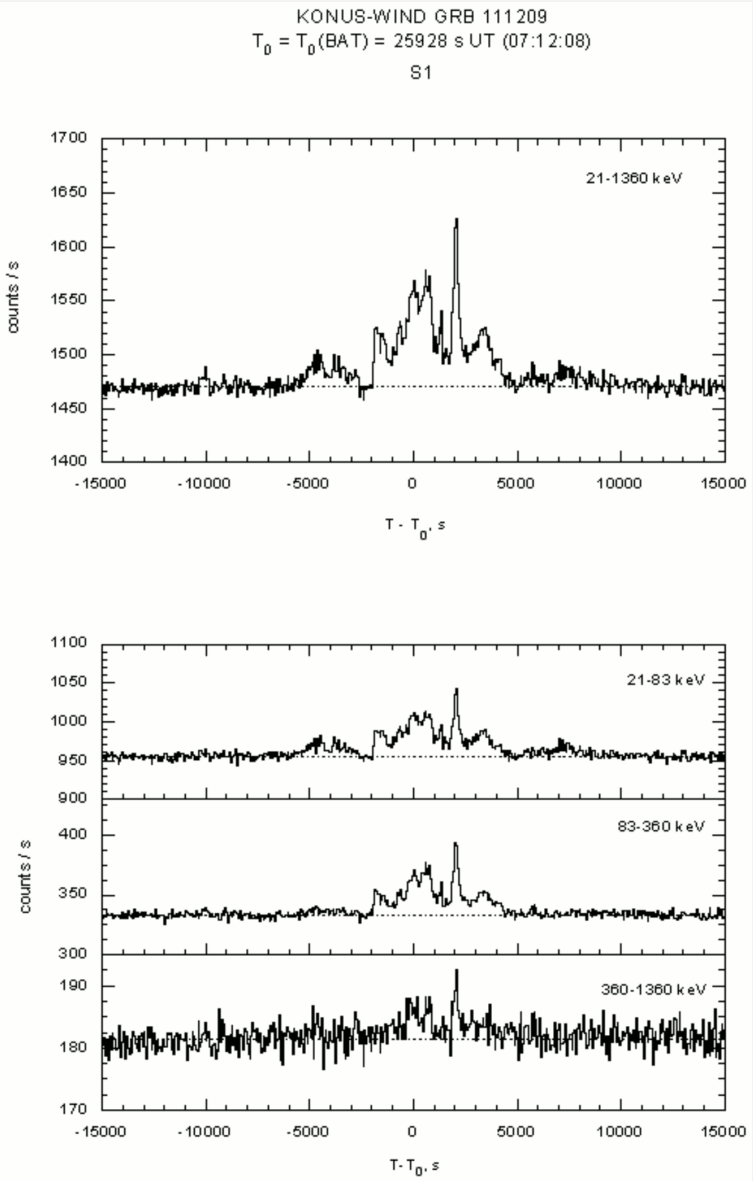

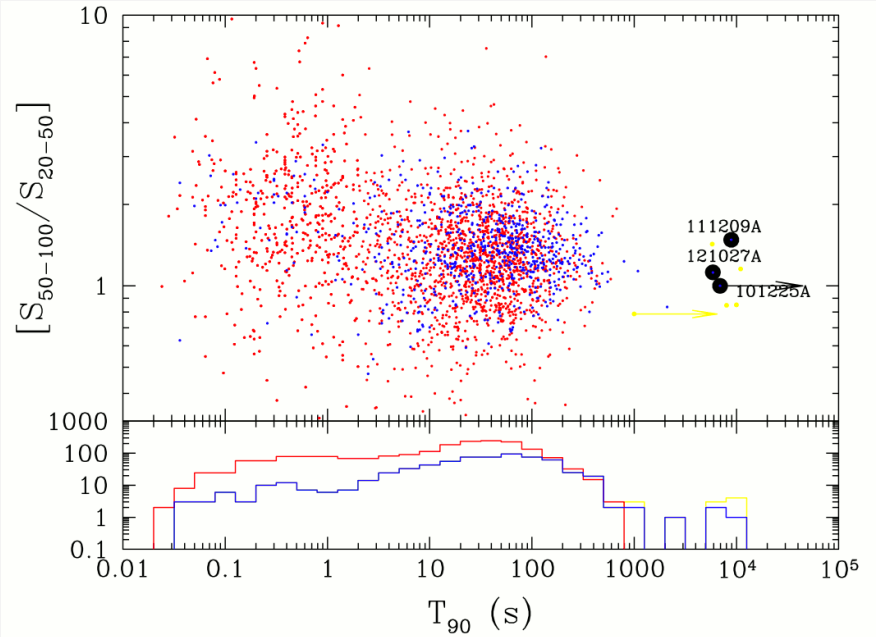

Figure 1. Spectral hardness (ratio of fluence in 50–100 keV over 20–50 keV) vs. duration diagram for *CGRO*/BATSE GRBs (red points) and *Swift* GRBs (blue points), with the locations of GRB 101225A, GRB 111209A, and GRB 121027A marked (note that these are approximate due to the lack of *Swift* orbit coverage). These three events have durations much longer than any seen by BATSE. In the case of GRB 101225A, the long-lived, low-level emission could easily have been missed, while GRB 111209A was seen as an extremely long burst by Konus-*WIND*. We also mark in yellow the location of other candidate ultra-long GRBs, in which the duration has been ascertained by the proxy of the time, or limits, on the rapid decay observed in the *Swift* XRT light curves. The lower panel shows a histogram of the observed durations, clearly identifying the location of the ultra-long bursts.

Levan et al. 2014

Ultra-Long GRBs

- Light curve of Ultra-long GRBs markedly different from that LGRBs
- Continuous activity up to late time
- “normal” afterglow decay after >> 10ksec

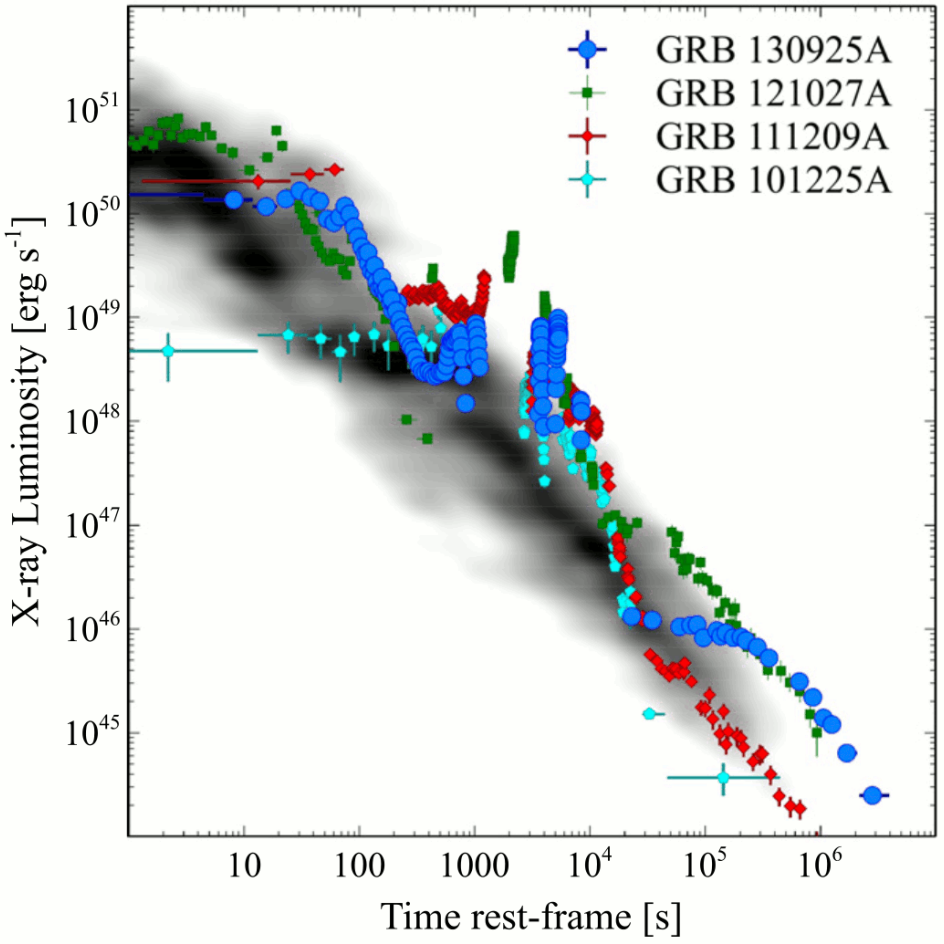

Figure 1. X-ray luminosity light curves for ultralong GRBs: GRB101225A at $z = 0.84$, GRB111209A at $z = 0.67$, GRB121027A at $z = 1.773$, and GRB 130925A at $z = 0.35$. The gray area shows the light curves of ~200 *Swift* long GRBs with measured redshift. The canonical (steep-flat-normal) afterglow decay can be recognized. Ultralong GRBs display continuous prompt emission activity up to late times, when standard long GRBs already follow the “normal” afterglow decay phase.

Piro et al. 2014

Non-GRB Events: Soft-Gamma Repeaters and Tidal Disruption Events

Soft-Gamma Repeaters

- Caused by **magnetars** emitting bright, repeating flashes of soft gamma rays.
- Fast rotating neutron stars (Galactic) with extraordinarily strong magnetic field of 10^{14}-10^{15} Gauss.
- e.g. SGR 1806-20, SGR 1900+14, SGR 1801-23, SGR 1627-41
- SGR 1900+14 on 27-12-2004:
  - Peak luminosity 10^{47} erg.s^{-1}.cm^{-2} at 15 kpc
  - Total energy output 10^{46} erg (solar output over 100 Myr)
  - Similar bursts would be detectable out to 40 Mpc (≈ distance to closest localized GRB)
  - Recurrence time long (~50 yr)

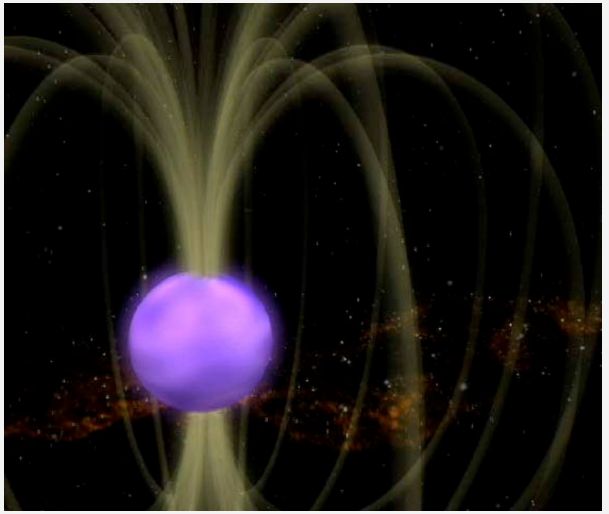

Artist's impression

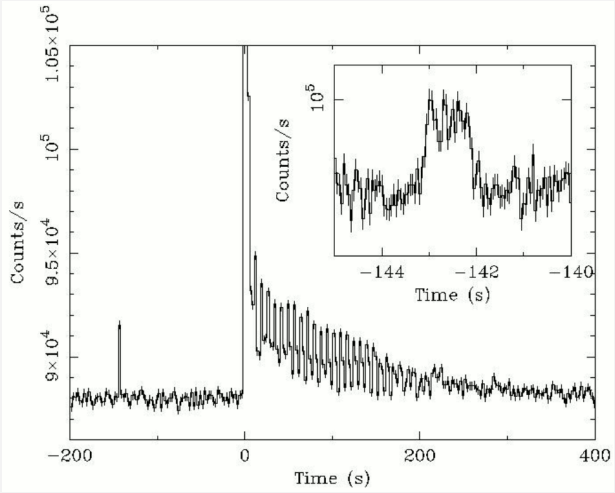

Long time scale light curve with saturated peak of SGR 1900+14 outburst observed by Ulysses in the 20-150 keV (Hurley et al. 2005).

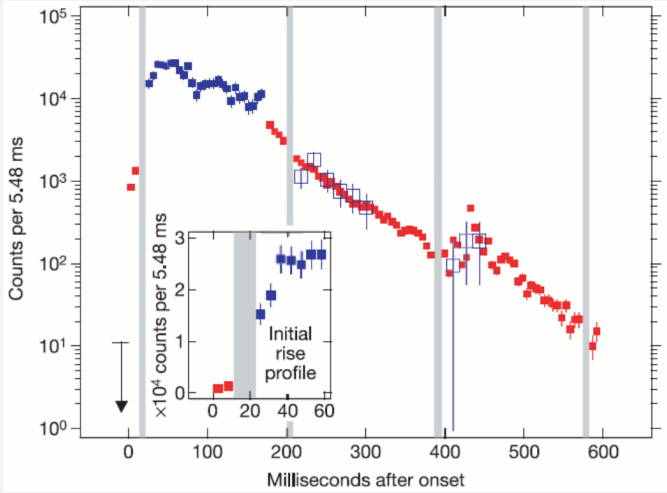

Light curve unsaturated peak, 4 orders of magnitude decay within 1 s (Terasawa et al. 2005).

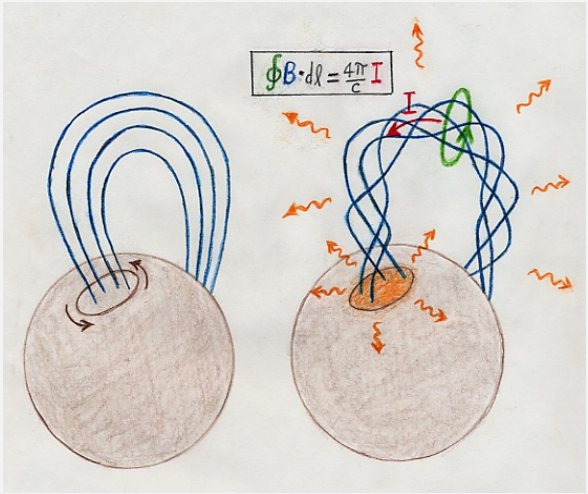

Robert Duncan web site on magnetars

Soft-Gamma Repeaters

- Magnetar distribution in our galaxy
- All but two (LMC, SMC) are Milky Way sources

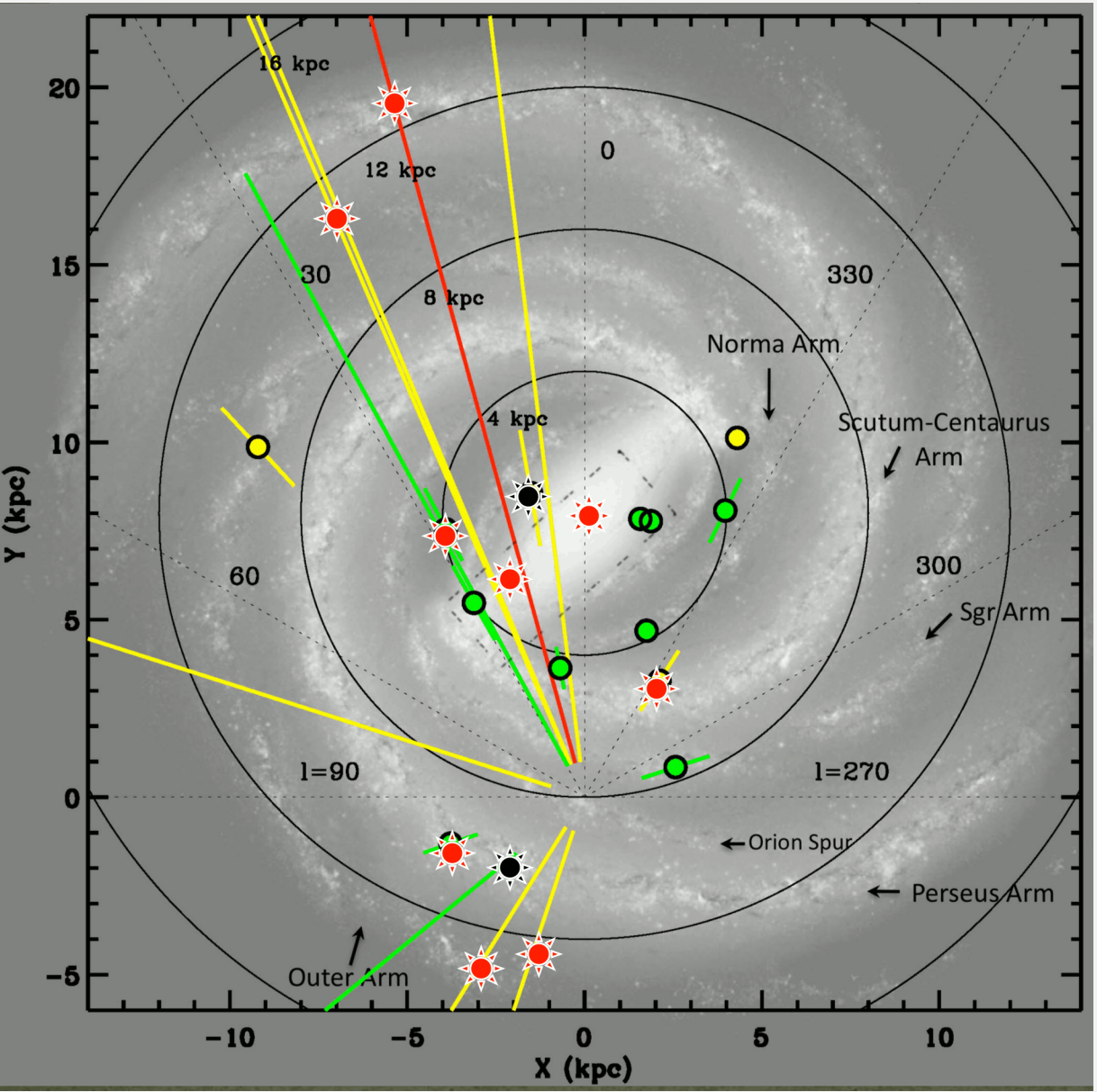

Detected with: Swift, Fermi, XMM, CXO, IPN, RXTE, PARKES

Old source reactivation

SGRs

AXPs (Anomalous X-ray Pulsars)

Kouveliotou et al. 2011

Tidal Disruption Events (TDE)

- Basic ideas developed in the ’80 (Rees 1989, Carter & Luminet 1982, Lacy, Townes & Hollenbach 1982)
- Super-massive BH + Main Sequence star
- Few candidates discovered mostly as X-ray flares (e.g. Komossa & Bade 1999)
- In most cases, a TDE is identified by
  - Having ~ $t^{5/3}$ decay in at least one wavelength
  - Occuring in the nucleus of a galaxy
- TDE can produce jets (e.g., Swift J1644)

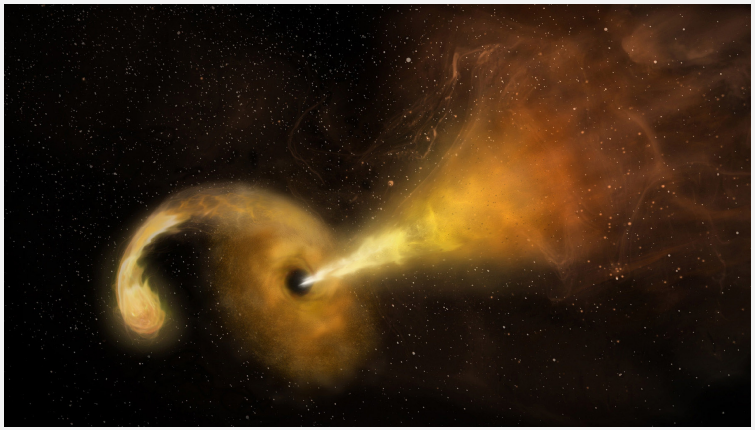

Artist's impression

Cannizzo, Troja & Lodato (2011)

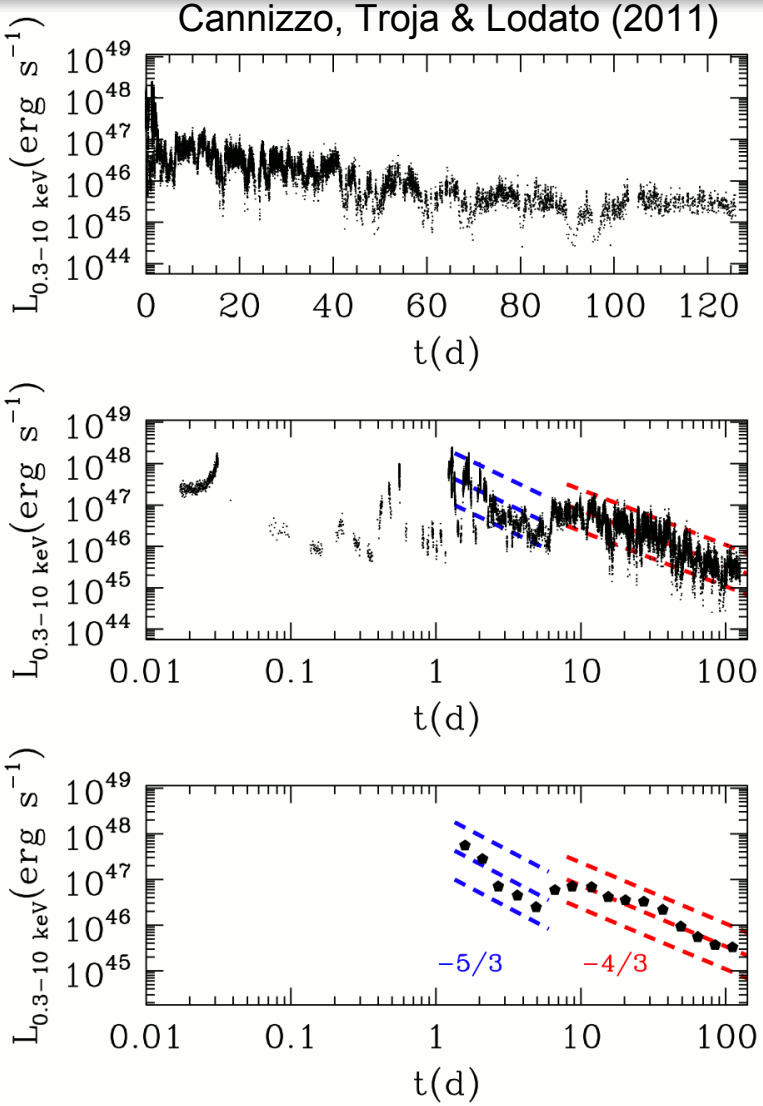

Figure 1. *Swift*/XRT light curve (Evans et al. 2007, 2009) for Sw 1644+57, plotted on both a log-linear (first panel) and log–log scale (second and third panels). In the third panel, we show the block averages of the X-ray flux, binned in time in 0.125 dex bins. The blue lines indicate the putative stellar debris fallback slope −5/3 and the red lines show the fallback decline rate expected due to a super-Eddington slim disk, −4/3. The data do not strongly support either decay law in detail, but are suggestive.

Kilonova (Macronova) and GW170817 / GRB 170817A

Kilonova (Macronova)

- Also called a macronova or r-process supernova.
- Merger of two NS, progenitor of SGRBs
- Strong electromagnetic radiation due to the radioactive decay of heavy r-process elements (rapid neutron capture) that are produced and ejected almost isotropically during the merger process.
- Red kilonova is expected from lanthanide-rich dynamical ejected via processes such as tidal forces.
- Blue kilonova could be due a lanthanide-poor wind driven outflow or cooling of shock-heated ejecta.
- Li & Paczynski 1998; Rosswog et al. 1999; Freiburghaus et al. 1999

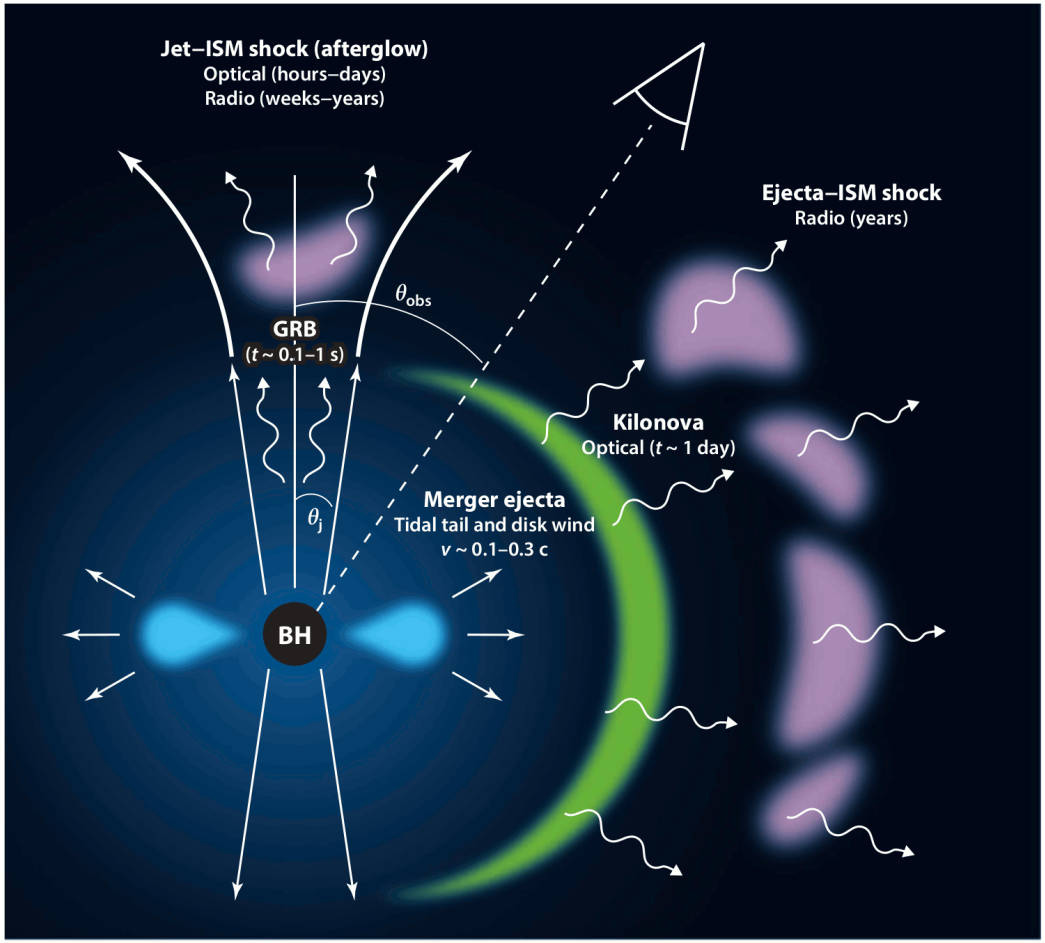

Metzger et al. 2010

Figure 20

Potential electromagnetic counterparts of compact object binary mergers as a function of the observer viewing angle (θ_{obs}). Rapid accretion of a centrifugally supported disk (*blue*) powers a collimated relativistic jet, which produces a short GRB. Owing to relativistic beaming, the gamma-ray emission is restricted to observers with $\theta_{obs} \lesssim \theta_j$. Afterglow emission results from the interaction of the jet with the circumburst medium (*pink*). Optical afterglow emission is detectable for observers with $\theta_{obs} \lesssim 2\theta_j$. Radio afterglow emission is observable from all viewing angles once the jet decelerates to mildly relativistic velocities on a timescale of months-years and can also be produced on timescales of years from subrelativistic ejecta. Short-lived isotropic optical/near-IR emission lasting a few days (kilonova; *green*) can also accompany the merger, powered by the radioactive decay of *r*-process elements synthesized in the ejecta. Reprinted from Metzger & Berger (2012) with permission.

Kilonova (Macronova)

- Mergers of NS-NS or NS-BH expected to create significant quantities of neutron-rich radioactive isotopes whose decay should result in a faint transient, known as a ‘kilonova’, in the days following the burst.
- Kilonova candidate GRB 130603B.

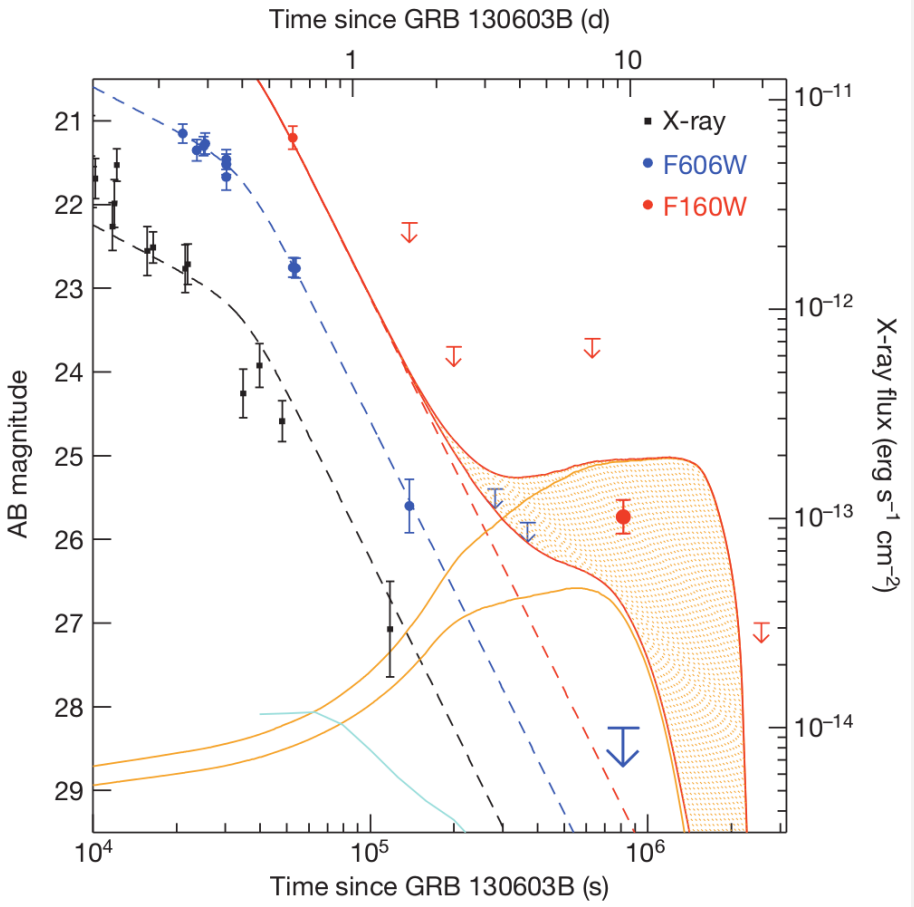

Figure 2 | Optical, NIR and X-ray light curves of GRB 130603B. Left axis, optical and NIR; right axis, X-ray. Upper limits are 2σ and error bars are 1σ. The optical data (g, r and i bands) have been interpolated to the F606W band and the NIR data have been interpolated to the F160W band using an average spectral energy distribution at ~0.6 d (Supplementary Information). HST epoch-1 points are given by bold symbols. The optical afterglow decays steeply after the first ~0.3 d and is modelled here as a smoothly broken power law (dashed blue line). We note that the complete absence of late-time optical emission also places a limit on any separate ^{56}Ni-driven decay component. The 0.3–10-keV X-ray data[29] are also consistent with breaking to a similarly steep decay (the dashed black line shows the optical light curve simply rescaled to match the X-ray points in this time frame), although the source had dropped below Swift sensitivity by ~48 h after the burst. The key conclusion from this plot is that the source seen in the NIR requires an additional component above the extrapolation of the afterglow (red dashed line), assuming that it also decays at the same rate. This excess NIR flux corresponds to a source with absolute magnitude $M(J)_{AB} \approx -15.35$ mag at ~7 d after the burst in the rest frame. This is consistent with the favoured range of kilonova behaviour from recent calculations (despite their known significant uncertainties[11–13]), as illustrated by the model[11] lines (orange curves correspond to ejected masses of 10^{-2} solar masses (lower curve) and 10^{-1} solar masses (upper curve), and these are added to the afterglow decay curves to produce predictions for the total NIR emission, shown as solid red curves). The cyan curve shows that even the brightest predicted r-process kilonova optical emission is negligible.

Tanvir et al. 2013

GW170817 / GRB 170817A

- EM counterpart from NS-NS merger event GW170817/GRB170817A.
- Large campaign of follow-up observations identified a kilonova.

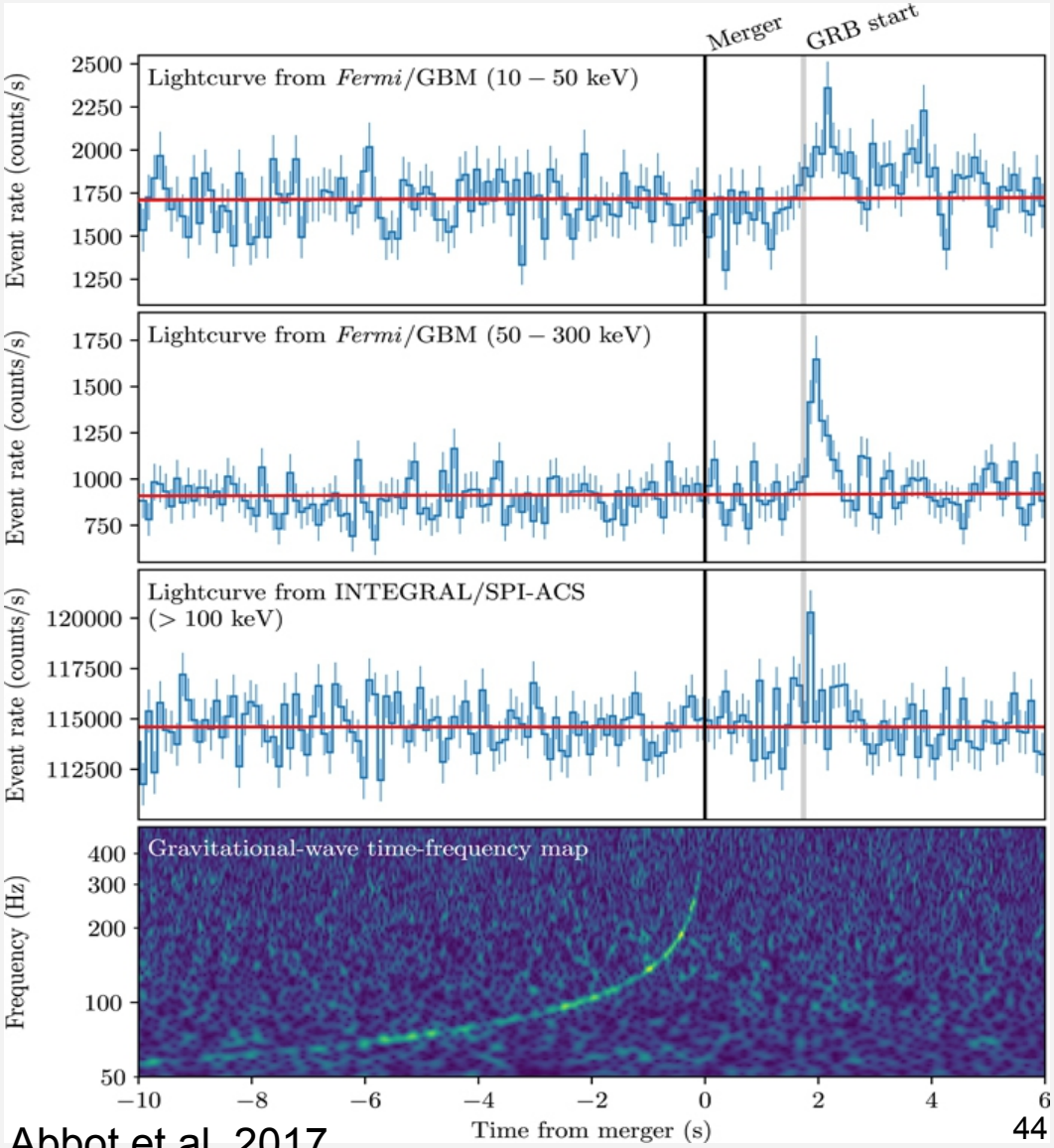

Abbot et al. 2017

GW170817 / GRB 170817A

Duration/Hardness

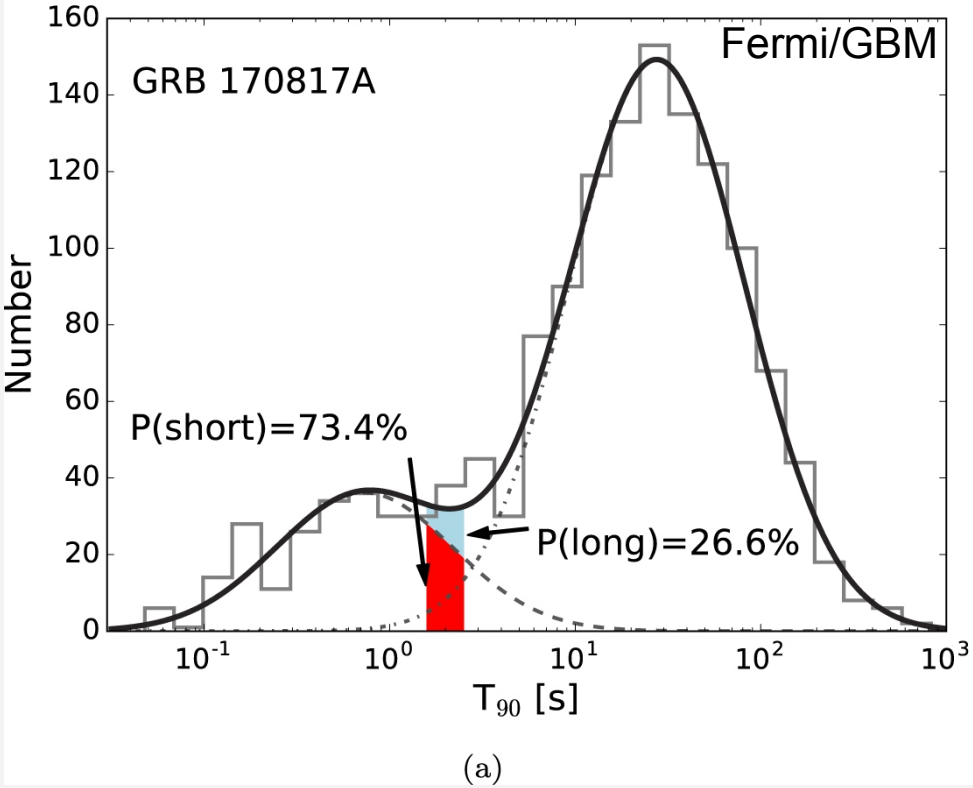

(a)

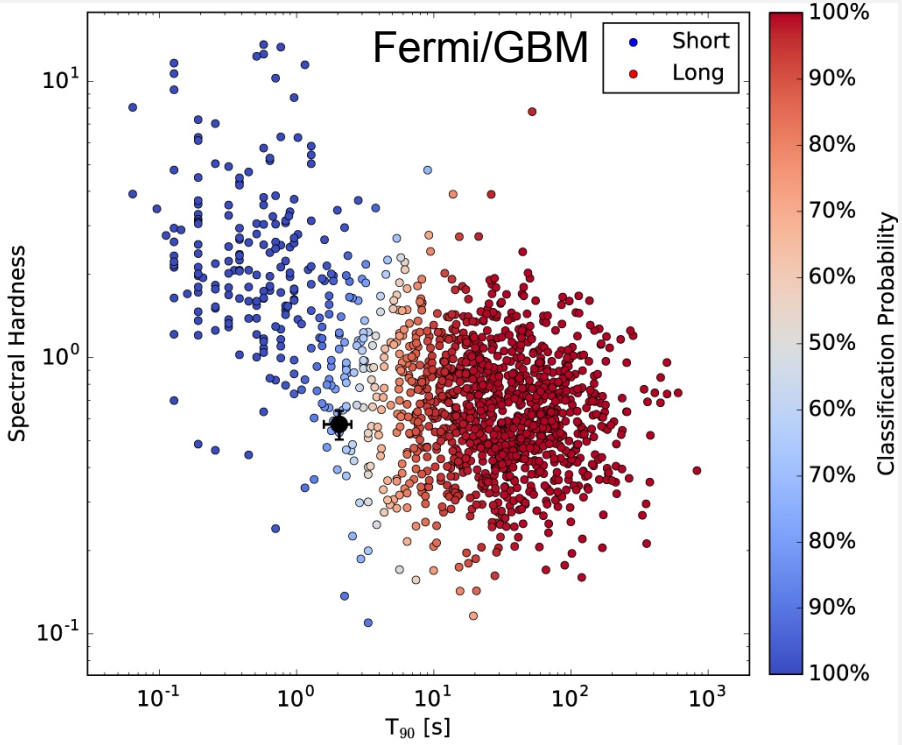

(b) Goldstein et al. 2017

- A standard catalog analysis using 50-300 keV range yields a T_{90} = 2.0 ± 0.5
- Combining both the duration and hardness information, gives P_{short} = 73.4%
- Hardness ratio between the 50-300 keV and 10-30 keV counts yields a relatively soft burst.

GW170817 / GRB 170817A

Hard Pulse and Soft Thermal Tail

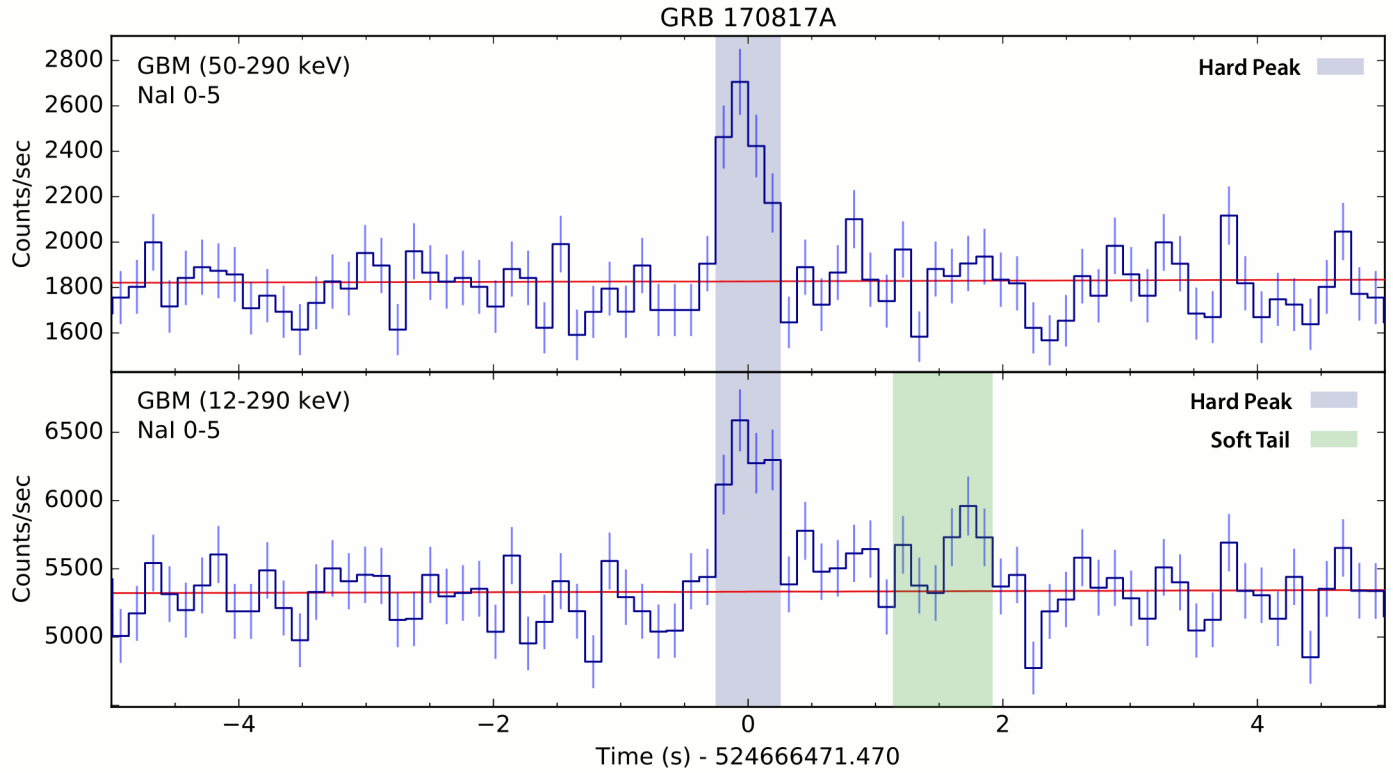

D. Kocevski

- Burst appears as a single component in the 50-300 keV energy range.
- Two components emerge when including photons in the 10-50 keV energy range.
- Initial hard pulse with a delayed and much softer tail.

Spectral Properties

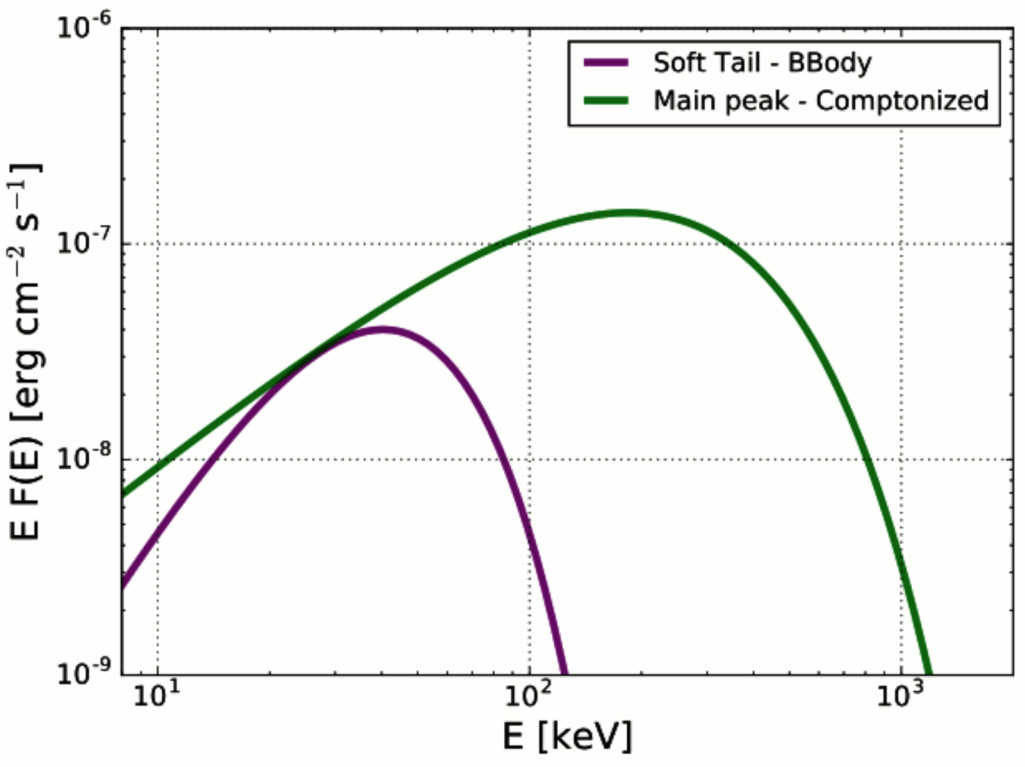

D. Kocevski

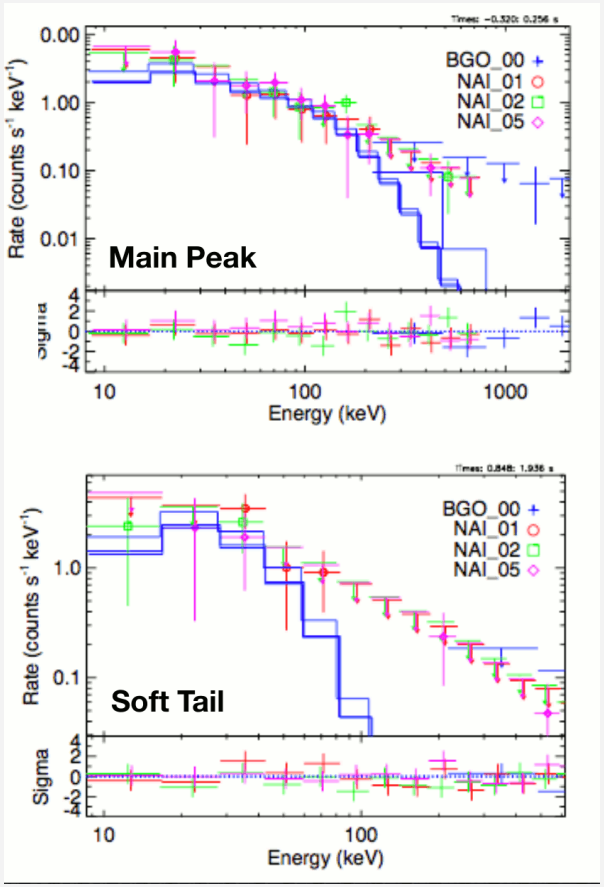

Goldstein et al. 2017

- The main hard peak is best fit with a Comptonized model with E_{peak} = 185 ± 62 keV.
- The soft tail is best fit by a black body with kT = 10.3 ± 1.5 keV.

Source Frame Energetics

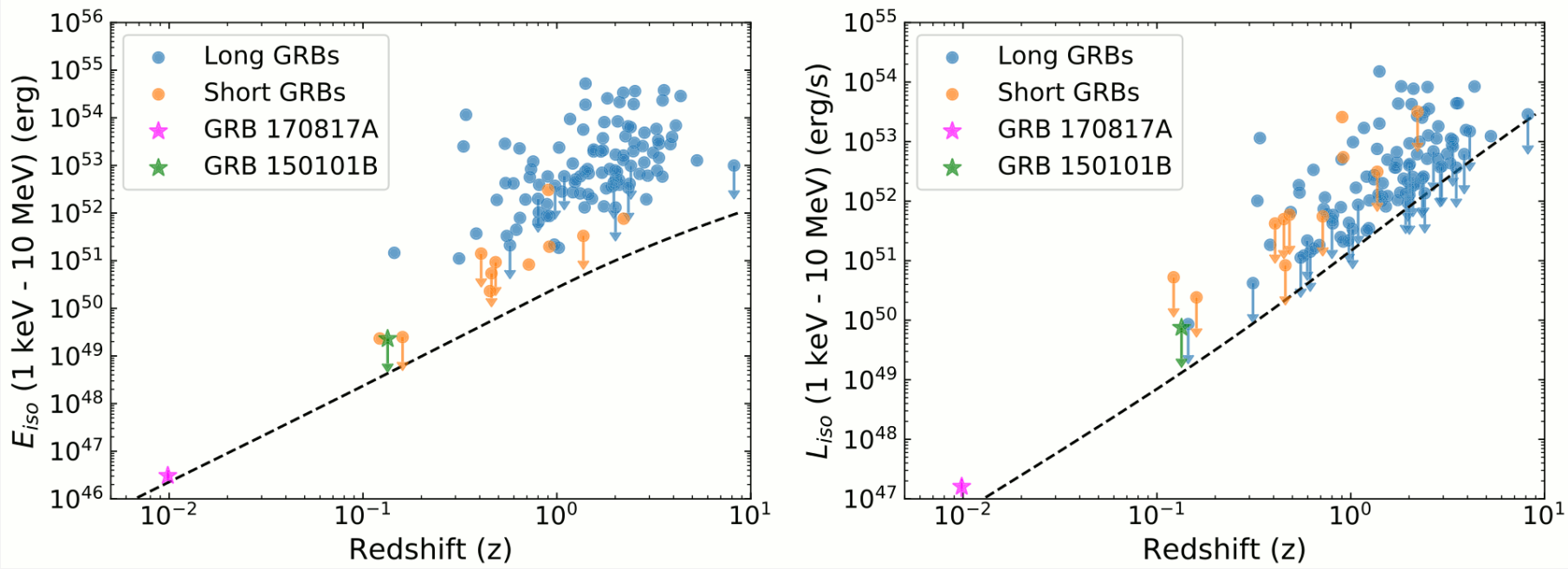

Burns et al. 2018

- GRB 170817A was extremely under luminous compared to other GRBs.
- It was one of the closest and least luminous GRBs ever detected.
- Estimated isotropic-equivalent energy is ~2-3 orders of magnitude lower than previous observations.

GW170817 / GRB 170817A

Localization

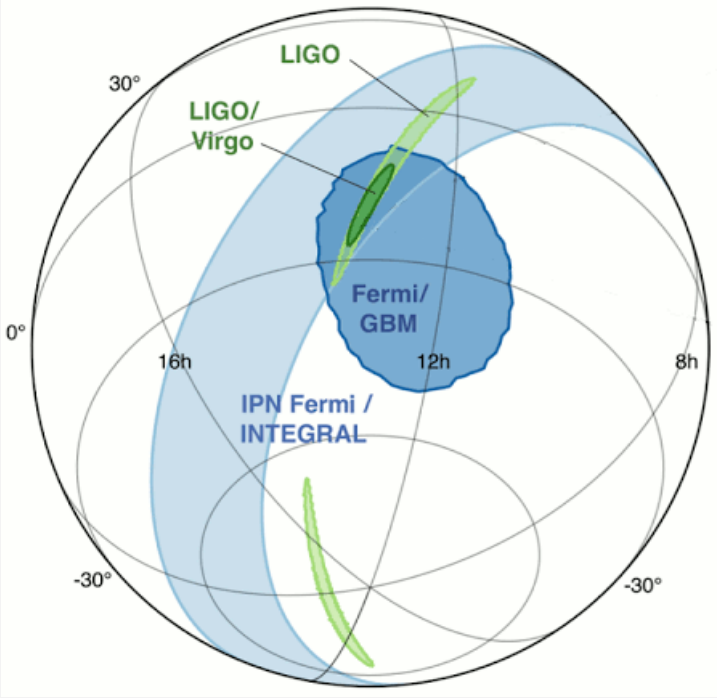

Localization of the gravitational-wave, gamma-ray, and optical signals. The left panel shows an orthographic projection of the 90% credible regions from LIGO (190 deg2; light green), the initial LIGO-Virgo localization (31 deg2; dark green), IPN triangulation from the time delay between Fermi and INTEGRAL (light blue), and Fermi-GBM (dark blue).

Abbott et al. 2017

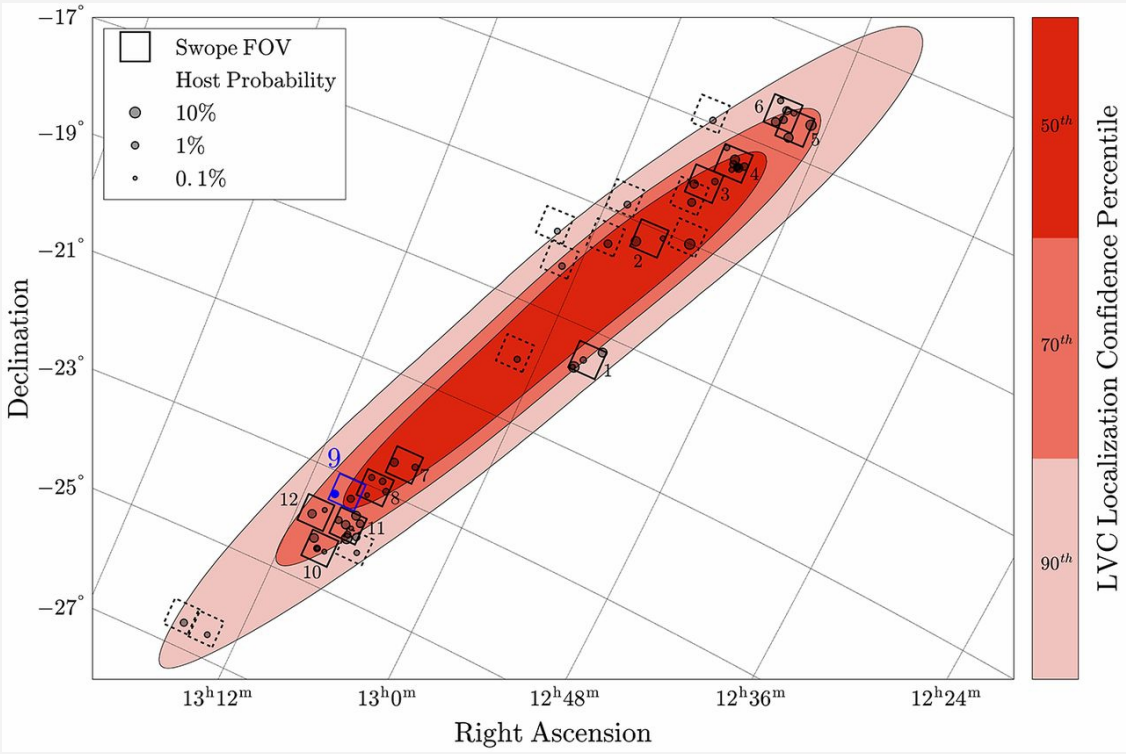

Sky region covering the 90th-percentile confidence region for the location of GW170817. Grey circles represent the locations of galaxies in our galaxy catalog and observed by the Swope telescope on 2017 August 17-18 to search for the EM counterpart to GW170817. The size of the circle indicates the probability of a particular galaxy being the host galaxy for GW170817. The square regions represent individual Swope pointings with the solid squares specifically chosen to contain multiple galaxies (and labeled in the order that they were observed) and the dotted squares being pointings which contained individual galaxies. The blue square labeled '9' contains NGC 4993, whose location is marked by the blue circle, and SSS17a.

Coulter et al. 2017

GW170817 / GRB 170817A

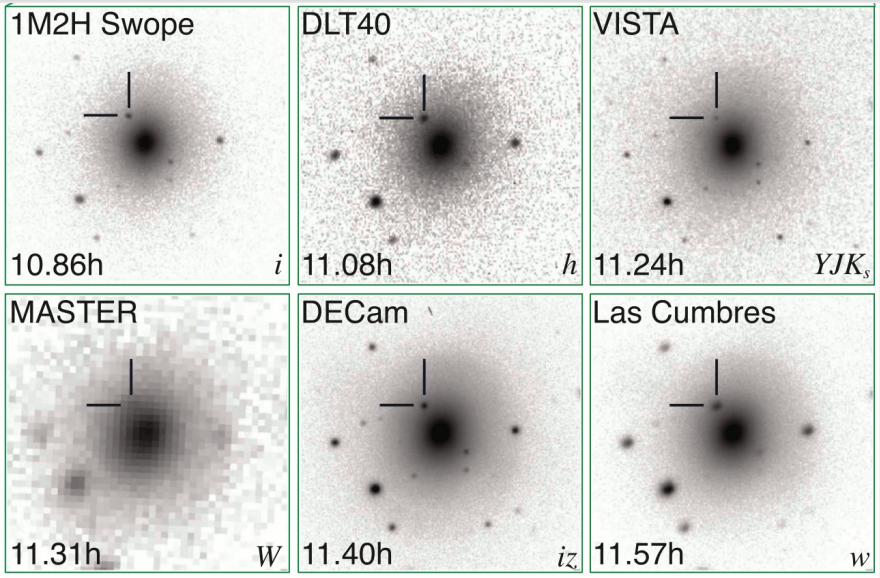

Reports of a blue optical transient near an elliptical S0 type galaxy NGC 4993 at ~40 Mpc (Abbot et al. 2017). Coulter et al. (2017) observed the region with the 1m Swope telescope at Las Campaas Observatory.

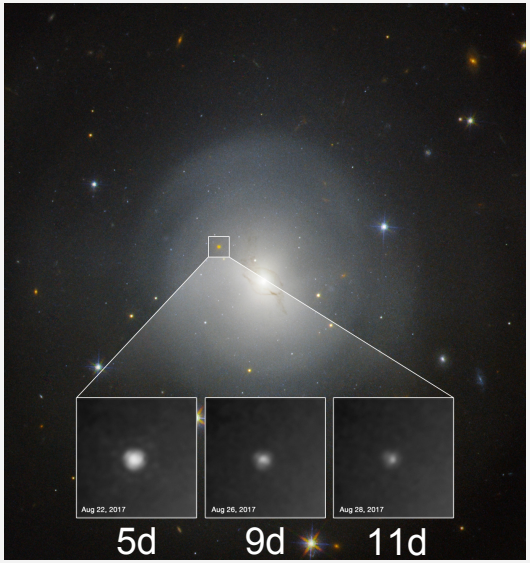

Image of galaxy NGC 4993 by Hubble Space Telescope. The kilonova was gradually fading over six days (Adams et al. 2017).

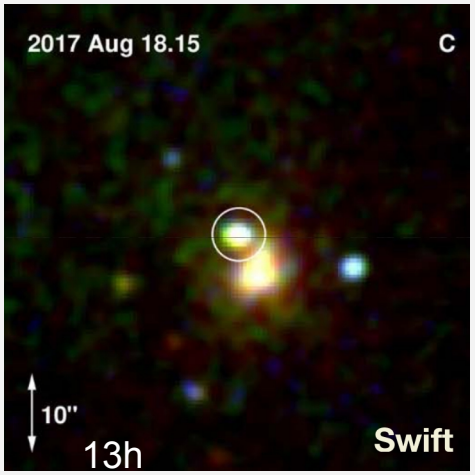

Swift observations reveal bright, but quickly fading, UV source with no evidence of X-ray emission (Evans et al. 2017).

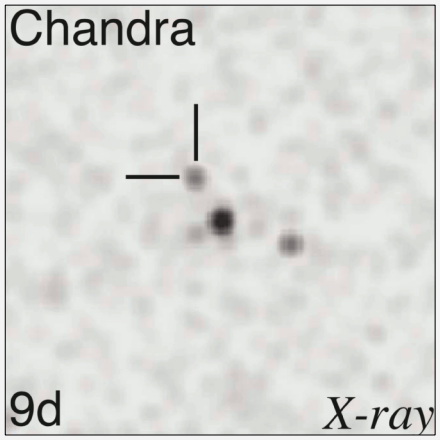

Chandra observations reveal first evidence of delayed X-ray emission (Troja et al. 2017).

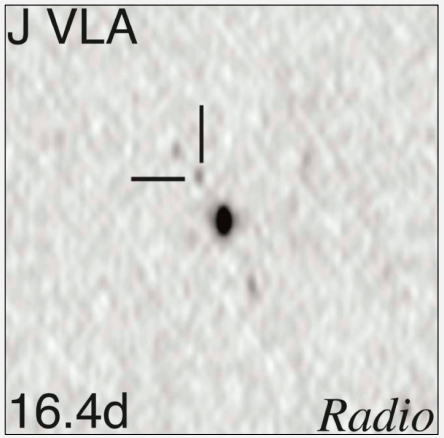

Radio counterpart reported by VLA (Mooley et al. 2017)

GW170817 / GRB 170817A

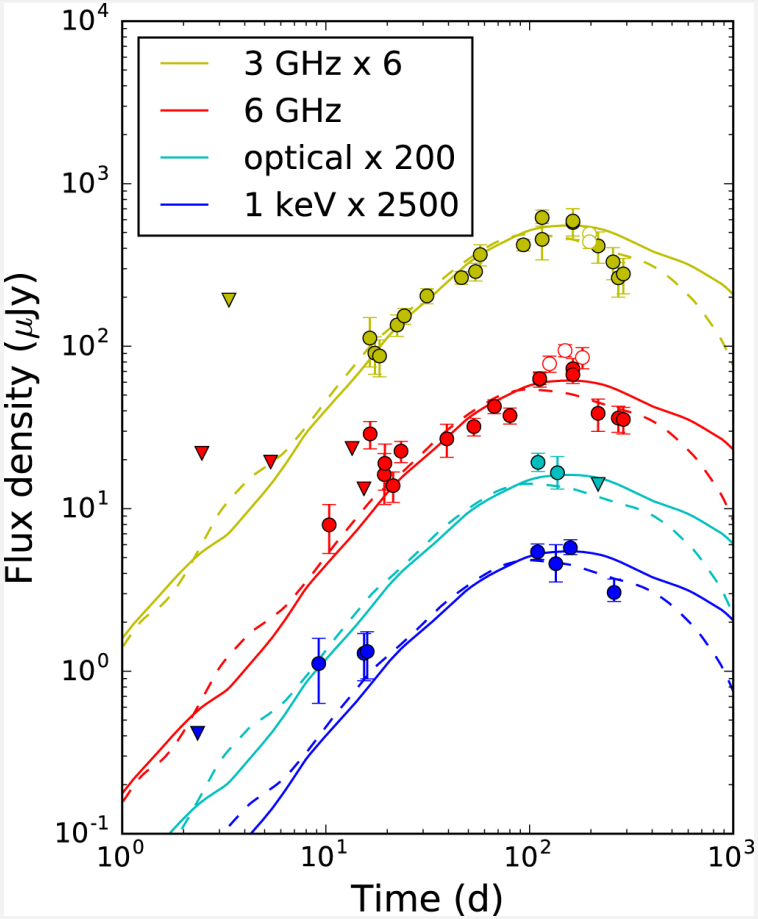

Alexander et al. 2018

Rising afterglow flux and a turn over in X-ray, optical and radio light curves of GW170817 (solid circles; open circles are the new data presented in Dobie et al. 2018). The data are clearly indicative of a decline at gsim200 days. Also shown are our structured jet models from Margutti et al. (2018); see Xie et al. (2018) for full details of the simulations.

GW170817 / GRB 170817A

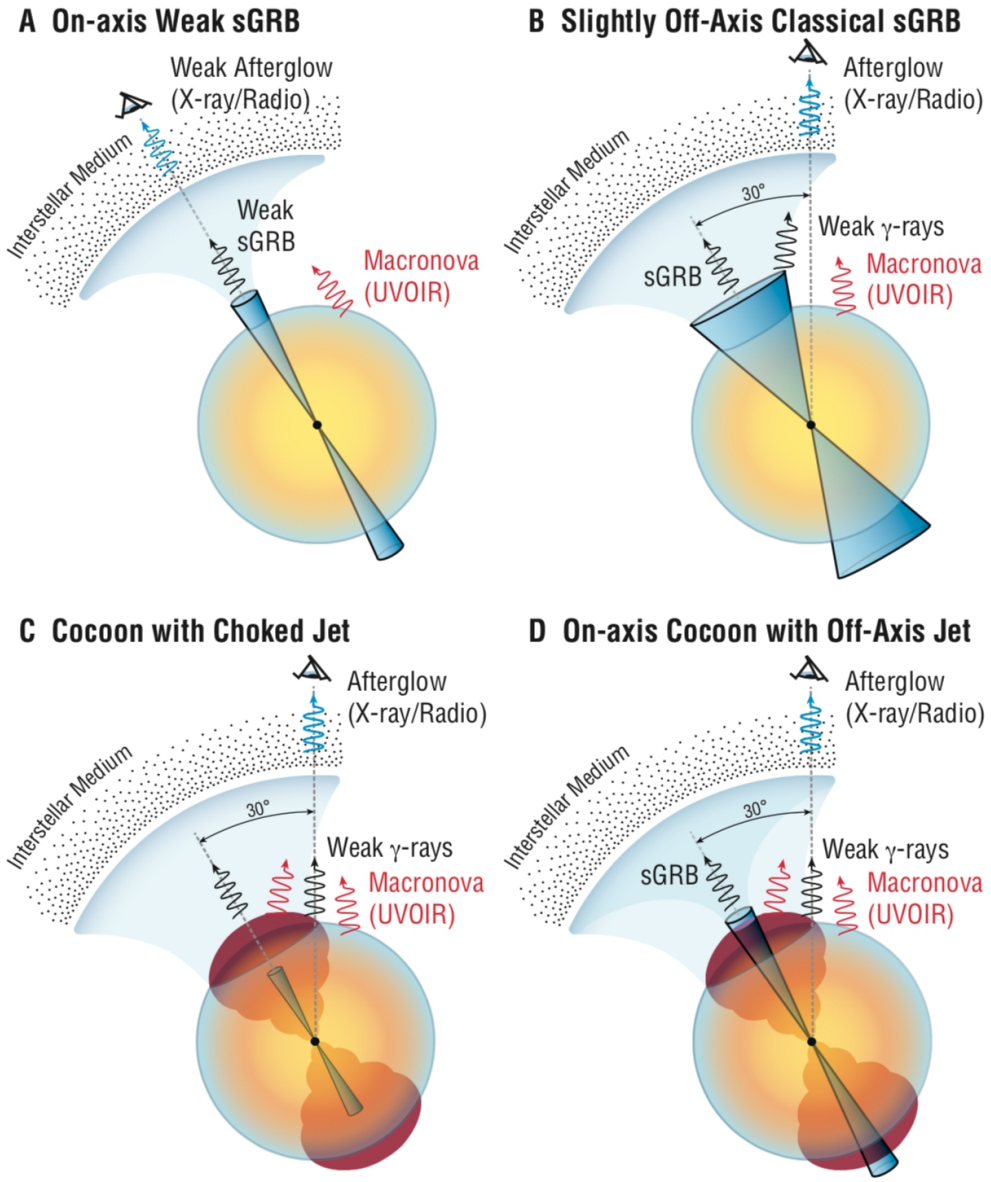

Kasliwal et al. 2017

- Many models are under discussion:
  - Off-axis GRB (Ioka & Nakamura et a. 2017)
  - Cocoon emission with successful or structured jet (Kasliwal et al. 2017, Mooley et al. 2017),
  - Scattered emission (Kisaka et al. 2017), etc.